Title
A Parmetric Study of Platoon Dynamics and Robust H[infinity] Controller Design

Authors
Oh, Pahngroc
Packard, Andy
Tongue, Benson H.

Publication Date
1999-11-01

CALIFORNIA PATH PROGRAM
INSTITUTE OF TRANSPORTATION STUDIES
UNIVERSITY OF CALIFORNIA, BERKELEY

A Parmetric Study of Platoon Dynamics and Robust H∞ Controller Design

Pahngroc Oh, Andy Packard, Benson H. Tongue

California PATH Research Report
UCB-ITS-PRR-99-40

This work was performed as part of the California PATH Program of the University of California, in cooperation with the State of California Business, Transportation, and Housing Agency, Department of Transportation; and the United States Department of Transportation, Federal Highway Administration.

Report for MOU 316

November 1999

ISSN 1055-1425

Final Report - Control of Heterogeneous Platoons

Pahngroc Oh, Andy Packard, and Benson H. Tongue
Department of Mechanical Engineering
University of California at Berkeley

California PATH Program

Abstract

A comprehensive simulation capability is presented for the analysis of vehicular platoons with or without collisions. **A** separate collision module (CDM) is integrated within the Platoon Simulation Package (PSP) to allow the recognition and dynamic simulation **of** intra-platoon collisions. Test simulations are presented and an alternative control strategy, one based on H_∞ optimization, is described. **This** control approach allows an explicit account to be taken unknown disturbances and system variations, i.e. it produces a robust design.

*keywords: PSP, **CDM,** ACI, performance, safety, **AHS,** H_∞*

Nomenclature

A	vehicle frontal area (m^2)
a_h	tire hysteresis (N/m)
c_b	bumper damping constant (Ns/m).
$c_{b,f}$	linear damping constant in front vehicle (Ns/m).
$c_{b,r}$	linear damping constant in rear vehicle (Ns/m).
$C_{b,f}$	maximum damping force in front vehicle bumper (N).
$C_{b,r}$	maximum damping force in rear vehicle bumper (N).
C_a	aerodynamic drag coefficient
$C_{a,un}$	percent uncertainty in aerodynamic drag coefficient
CR_r	correction factor for rolling resistance uncertainty bounds
e_{ff}	drivetrain effectiveness, percent
e_{un}	percent uncertainty in engine effectiveness
F	total force acting on a car (N)
F_a	aerodynamic drag force (N)
F_b	brake force acting at the tire-road interface (N)
F_{body}	force applied to vehicle body (N).
$F_{b,m}$	maximum brake force available at the tire-road interface (N)
F_e	engine force acting at the tire-road interface (N)
$F_{e,m}$	maximum engine force available at the tire-road interface (N)
F_g	gravitational force due to road grade (N)
F_r	rolling resistance force (N)
f_r	coefficient of rolling resistance
$f_{r,un}$	percent uncertainty in coefficient of rolling resistance
G_o	road roughness
GR	gear ratio reduction from engine shaft to wheel axle
g	gravitational acceleration (m/s^2)
h	axle height (tire radius) (m)
k_b	bumper spring constant (N/m).
$k_{b,f}$	bumper stiffness in front vehicle (N/m).
$k_{b,r}$	bumper stiffness in rear vehicle (N/m).
k_c	vehicle body spring constant (N/m).
$k_{c,f}$	body stiffness in front vehicle (N/m).
$k_{c,r}$	body stiffness in **rear** vehicle (N/m).
L_b	dead length of bumper (m).
L_c	active length of car body (m).
L_i	length of car i (m)
M	vehicle mass **(kg)**
M_{un}	percent uncertainty in vehicle mass

$PC(v)$	power curve function for engine torque (N·m)
S	spacing between car i and car $i-1$ (m)
S_d	desired spacing
T_b	brake torque (N·m)
$T_{b,m}$	maximum brake torque (N·m)
T_e	engine torque (N·m)
$T_{e,m}$	maximum engine torque (N·m)
TR	road traction
v	velocity of vehicle (m/s)
v_w	velocity of wind (m/s)
w	vehicle width (m).
α_b	brake input
δ	preload distance on car body spring (m).
Δ_i	space error between front of car i and back of car $i-1$ (m)
θ	road grade (rad)
μ	braking coefficient of friction
μ_{un}	percent uncertainty in braking coefficient of friction
ρ	density of air (kg/m^3)
τ_b	brake time lag (sec)
τ_e	engine time lag (sec)
ϕ	engine input
w	engine speed (RPM)

EXECUTIVE SUMMARY

This report details the development and implementation of a robust control design approach for platoons of vehicles. The motivation behind the development was the realization that system parameters will not be fixed in any real world platooning implementation and that controllers not designed with parametric variations in mind can behave in a markedly degraded fashion as compared with their performance under nominal condition if variations occur. The approach used in this report is well suited for systems in which parametric variations are expected to occur and will produce stable controllers that allow the system's performance to be relatively insensitive to variations in the operational parameters.

Contents

1 INTRODUCTION

Platooning in Automated Highway Systems (AHS) has been introduced as a means of addressing both traffic congestion and safety problems in the highway system. The basic idea of platooning is to keep a tight spacing between consecutive vehicles so as to increase the capacity of existing highways while simultaneously ensuring safety. Hence, in densely populated area, an existing highway could be used more effectively and could satisfy the future forecasted demand without the need for new highways. The development of advanced Automative Vehicle Control Systems (AVCS) is an essential first step towards the development of a viable **AHS.**

String stability is a key property in designing an AVCS since it ensures that errors decrease as they propagate down the platoon [28]. Sheikholeslam and Desoer showed that by using feedback linearization [17], a stable platoon can be achieved in the presence of perturbations in the vehicle's mass, even with communication delays and measurement noises. Unfortunately, their approach is not well suited for the case when each vehicle in the platoon has differing properties such as variable braking capabilities. We shall show that this difficulty can be ameliorated through the use of a robust H_∞ controller.

This report consists of two parts. In the first we discuss the Platoon Simulation Package (PSP) which has been developed in the Dynamics Systems Laboratory at the University of California at Berkeley [30, **33, 34, 35,** 36]. We integrated the vehicle Collision Dynamics Model (CDM) into the PSP to allow an examination of platoon dynamics with or without collisions. Although always undesirable, collisions play an important part in the ultimate decision of how and where platooning will take place. Multiple simulations using PSP with CDM can help researchers in understanding a platoon's behavior in different emergency scenarios and should help enable the design of safer platoons. Three collision severity measures are introduced in Section **3** and their relative merits discussed.

This report's second half focuses on the longitudinal control of each vehicle within a platoon. We first derive a third order linearized vehicle model, followed by an H_∞ optimization. Two control approaches, feedback linearization and robust H_∞, are compared for identical lead car information. To examine the effects on platoon behavior as a result of parameter variations, simulations were performed for a platoon consisting of four non-identical vehicles with different brake time constants. Simulation results show that the newly designed H_∞ controller results in a smaller spacing error than that found under feedback linearlization.

2 Platoon Simulation Package

In this section we describe how the Collision Dynamics Model (CDM) [32] is folded into the Platoon Simulation Package (PSP) [30] that has been developed to investigate the performance of a platoon of vehicles for Automated Highway Systems (AHS). Since the CDM module allows vehicle to vehicle contact, its inclusion in the PSP allows one to evaluate control approaches when collisions manifest themselves. The general model of a four-vehicle platoon is shown in Figure 1. Each vehicle has four states: position, velocity, engine and brake dynamics. The distances of the current vehicle's front body end, front bumper end and the preceding vehicle's rear from the current vehicle's mass center, and a collision flag are four states of CDM between ***cars.*** The only state of the lead car is its position. Hence, our four-vehicle platoon model has 29 states.

2.1 Platoon Configuration

The assumed platoon configuration is shown in Figure 2. From this, the kinematic equations for each vehicle can be deduced as follows:

$$\Delta_i(t) = x_{i-1}(t) - x_i(t) - S_d - L_i \qquad \text{for } i = 2, 3, \ldots \tag{1}$$

$$\Delta_1(t) = x_l(t) - x_1(t) - S_d - L_1 \tag{2}$$

where Δ_i denotes the spacing error between $(i-1)$th and i-th vehicles, x_i denotes the position of i-th vehicle, S_d denotes the desired spacing and L_i denotes i-th vehicle length.

2.2 Vehicle Model

Figure **3** shows the vehicle model of the i-th vehicle in the platoon. The acceleration of the vehicle in this model can be determined from Newton's second law:

$$m_i\ddot{x} = F_e - F_b - F_a - F_g - F_r \tag{3}$$

where F_e denotes the force produced by the powertrain, F_b denotes the braking force, F_a denotes the aerodynamic drag force, F_g denotes the gravitional force due to the road slope and F_r denotes the rolling resistance due to the deformation of wheel and road surface.

2.2.1 Powertrain model

The engine dynamics of the i-th vehicle is modeled **as**

$$\dot{\xi}_i = -\frac{\xi_i}{\tau_i(\dot{x}_i)} + \frac{u_i}{m_i\tau_i(\dot{x}_i)} \tag{4}$$

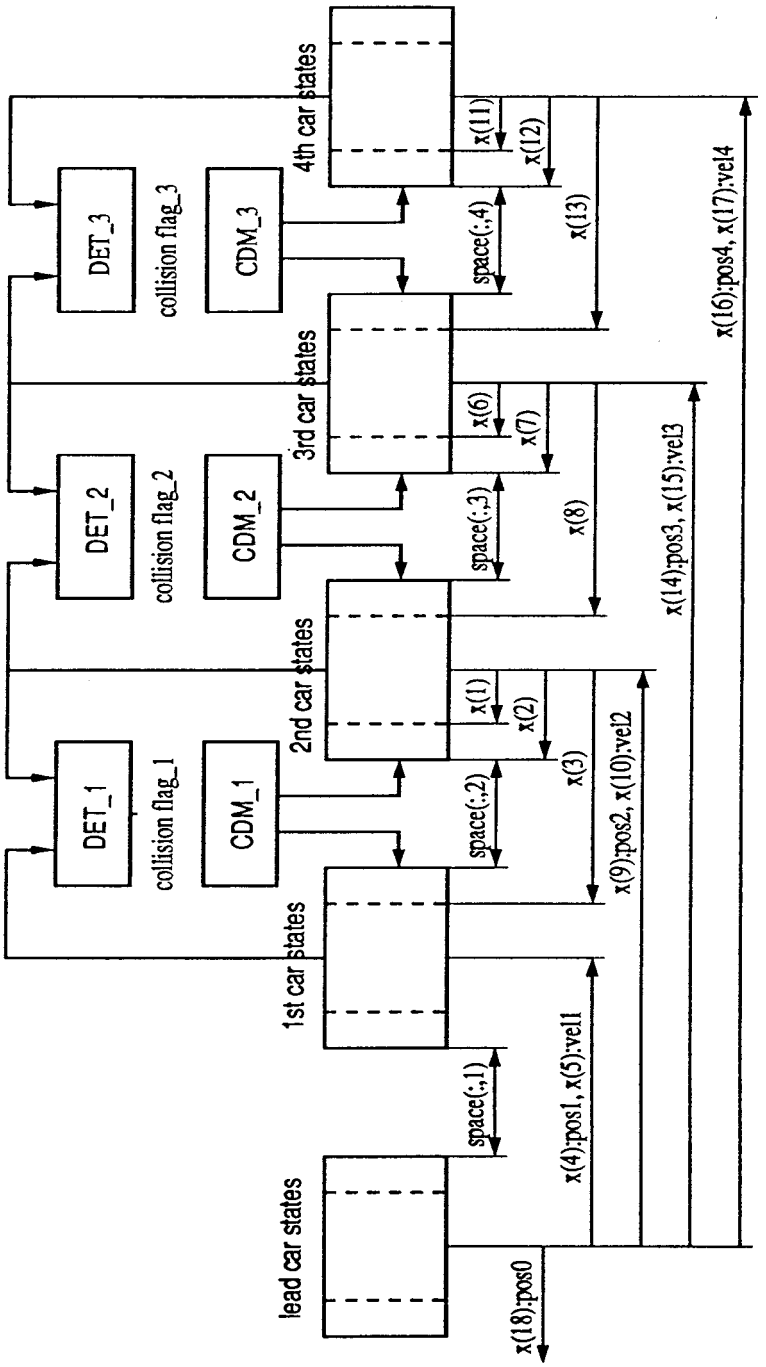

Figure 1: General Model of a Four Vehicle Platoon

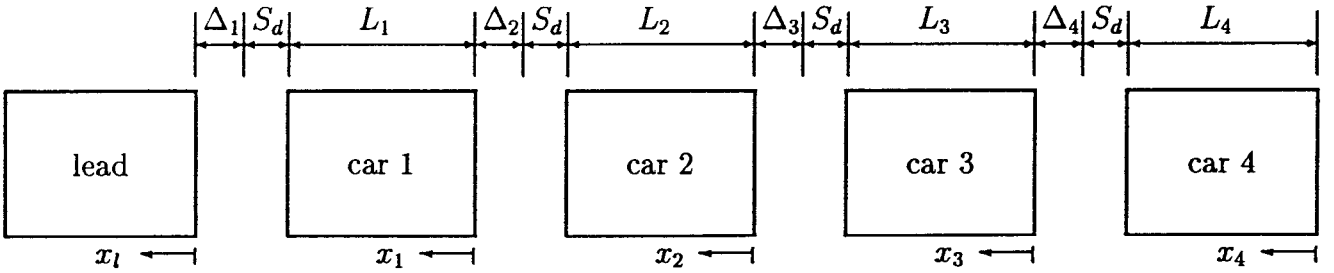

Figure **2:** Model of a 4car Platoon with Lead Car

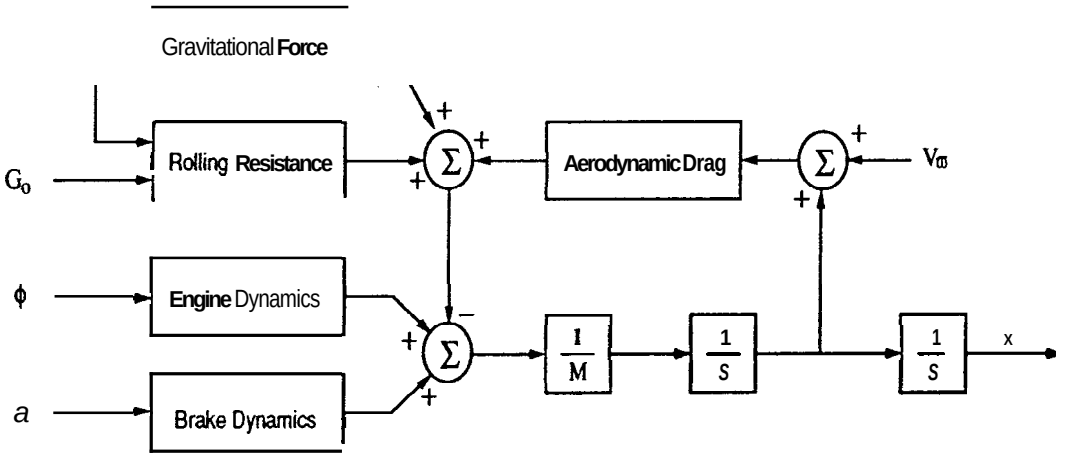

Figure **3:** Model of the i-th Vehicle in Platoon

where, $\tau_i(\dot{x}_i)$ denotes the i-th vehicle's engine time constant when the i-th vehicle is travelling with a speed equal to $\dot{x}_i$, u_i denotes the throttle input to the i-th vehicle's engine, and $F_i = m_i\xi_i$ denotes the traction force produced by the i-th vehicle's engine.

Tongue and Sachi suggested the use of an engine power curve relationship, which is usually given by automobile makers, in order to determine a saturation limit to the powertrain output followed by a first-order time lag [30]. Multiplying the maximum torque from the power curves by the gear ratios and drivetrain efficiency and dividing by the wheel base produces the maximum engine force transmitted through the tires:

$$F_{e,m} = PC(v) \cdot e_{ff} \cdot GR/h \tag{5}$$

where

$T_{e,m} = PC(\omega)$ (given by car manufacturers)
$w = v \cdot GR/h$

Adding a term for uncertainty in engine effectiveness yields:

$$F_{e,m} = PC(v) \cdot e_{ff} \cdot GR/h \,.(1 + e_{un}) \tag{6}$$

2.2.2 Brake model

A simple first order lag expression for braking force is [12]:

$$F_b = \alpha_b \cdot F_{b,m} \cdot (1 - e^{-\frac{t}{\tau_b}}) \tag{7}$$

where the simplified equation for the maximum braking force is given by:

$$F_{b,m} = \mu \cdot M \cdot g \cdot h \tag{8}$$

Including the parametric variations gives:

$$F_{b,m} = \mu \cdot (1 + \mu_{un}) \cdot M \cdot (1 + M_{un}) \cdot g \cdot h \tag{9}$$

2.2.3 Aerodynamic drag

The force due to aerodynamic drag is [29, 33]:

$$F_a = \begin{cases} 0 & \text{if } \Delta \leq .5H \\ .4(\Delta - .5H) \cdot C_a \cdot (v + v_w)^2 \cdot sgn(v + v_w) & \text{if } .5\text{H} < \mathbf{A} \leq 3\text{H} \\ C_a \cdot (v + v_w)^2 \cdot sgn(v + v_w) & \text{if } 3H > \mathbf{A} \end{cases} \tag{10}$$

where $C_a = \frac{\rho A C_d}{2}$ (ρ denotes the specific mass of air, A denotes the cross-sectional area of the vehicle, and C_d denotes the drag coefficient), H is the height of the front vehicle, v_w is the wind gust velocity and A is the headway spacing between vehicles.
Including terms in the above equation to account for parametric variations gives:

$$F_a = \begin{cases} 0 & \text{if } \mathbf{A} \leq .5\text{H} \\ .4(\Delta - .5H) \cdot C_a \,.(1 + C_{a,un}) \cdot (v + v_w)^2 \cdot sgn(v + v_w) & \text{if } .5H < \mathbf{A} \leq 3\text{H} \\ C_a \cdot (1 + C_{a,un}) \cdot (v + v_w)^2 \cdot sgn(v + v_w) & \text{if } 3H > \mathbf{A} \end{cases} \tag{11}$$

2.2.4 Rolling Resistance

Rolling resistance occurs when the tire and road surface deform. An approximate calculation of the rolling resistance can be made using the coefficient of rolling resistance. The force due to rolling resistance is:

$$F_r = M \cdot g \cdot f_r \cdot \cos(\theta) \tag{12}$$

where f_r denotes the coefficient of rolling resistance. The rolling resistance coefficients are a function of the vehicle velocity(v) as depicted in **ASTM STP884** [10], and the following curve-fit may be used [33]:

$$\begin{aligned} f_r &= (4.864 \times 10^{-4} \cdot G_o - 1.03 \times 10^{-8}) \cdot v^3 \\ &\quad +(-0.0952 \cdot G_o + 1.1425 \times 10^{-6}) \cdot v^2 \\ &\quad +(7.0982 \cdot G_o - 3.1010 \times 10^{-5}) \cdot v + 0.01 \end{aligned} \tag{13}$$

where

$$4.050 \times 10^{-7} \leq G_o \leq 6.400 \times 10^{-6} \text{ for highways}$$

The above equation can be rewritten in terms of tire hysteresis(a_h), axle height(h), correction factor(CR_r), and uncertainty in the coefficient of rolling resistance (which includes changes in G_o), the relationship for the coefficient of rolling resistance becomes [30]:

$$\begin{aligned} f_r &= \frac{a_h}{h} \cdot (-7.209 \times 10^{-14} \cdot v^3 + 7.877 \times 10^{-12} \cdot v^2 \\ &\quad -2.007 \times 10^{-10} \cdot v + 7.136 \times 10^{-8}) \cdot CR_r \cdot (1 + f_{r,un}) \end{aligned} \tag{14}$$

2.2.5 Gravitational force

The force due to road grade is:

$$F_g = \mathbf{M} \cdot g \cdot \sin(\theta) \tag{15}$$

Including parametric variations in M gives:

$$F_g = M \cdot (1 + M_{un}) \cdot g \cdot \sin(\theta) \tag{16}$$

2.3 Collision Dynamics Module (CDM) [32]

Figure **4** is a schematic of two car collision dynamics module. The model consists of three state equations and two output equations for each collision scenario. The CDM inputs are position and velocity of each vehicle and outputs to the **PSP** are dynamic forces acting on the vehicles due to the collision. The following equations govern the **CDM** during contact and non-contact situations.

- Bumpers dynamics active.
  - Both bumper dampers in linear region.

$$\begin{aligned} \dot{x_1} &= v_f \\ \dot{x_2} &= \frac{k_{b,f}(x_2 - x_1 - L_{b,f}) - k_{b,r}(x_3 - x_2 - L_{b,r}) - c_{b,f} v_f - c_{b,r} v_r}{-(c_{b,f} + c_{b,r})} \\ \dot{x_3} &= v_r \\ F_f &= k_{b,f}(x_2 - x_1 - L_{b,f}) + c_{b,f}(\dot{x_2} - \dot{x_1}) \\ F_r &= -k_{b,r}(x_3 - x_2 - L_{b,r}) - c_{b,r}(\dot{x_3} - \dot{x_2}) \end{aligned} \tag{17}$$

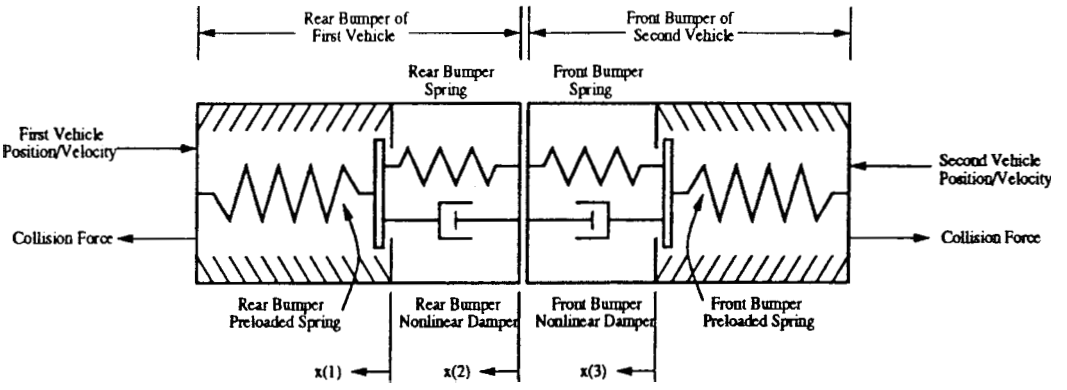

Figure **4:** Schematic of **Two** Car CDM

– Front vehicle bumper in linear region, rear vehicle bumper in constant region.

$$\begin{aligned} \dot{x_1} &= v_f \\ \dot{x_2} &= \frac{k_{b,f}(x_2 - x_1 - L_{b,f}) - k_{b,r}(x_3 - x_2 - L_{b,r}) - c_{b,f}v_f - C_{b,r}}{-c_{b,f}} \\ \dot{x_3} &= v_r \\ F_f &= k_{b,f}(x_2 - x_1 - L_{b,f}) + c_{b,f}(\dot{x_2} - \dot{x_1}) \\ F_r &= -k_{b,r}(x_3 - x_2 - L_{b,r}) + C_{b,r} \end{aligned} \tag{18}$$

– Front vehicle bumper in constant region, rear vehicle bumper in linear region.

$$\begin{aligned} \dot{x_1} &= v_f \\ \dot{x_2} &= \frac{k_{b,f}(x_2 - x_1 - L_{b,f}) - k_{b,r}(x_3 - x_2 - L_{b,r}) - C_{b,f} - c_{b,r}v_r}{-c_{b,r}} \\ \dot{x_3} &= v_r \\ F_f &= k_{b,f}(x_2 - x_1 - L_{b,f}) - C_{b,f} \\ F_r &= -k_{b,r}(x_3 - x_2 - L_{b,r}) - c_{b,r}(\dot{x_3} - \dot{x_2}) \end{aligned} \tag{19}$$

– Both vehicle bumpers in constant region.

$$\begin{aligned} \dot{x_1} &= v_f \\ \dot{x_2} &= \frac{k_{b,f}v_f + k_{b,r}v_r}{k_{b,f} + k_{b,r}} \\ \dot{x_3} &= v_r \\ F_f &= k_{b,f}(x_2 - x_1 - L_{b,f}) - C_{b,f} \\ F_r &= -k_{b,r}(x_3 - x_2 - L_{b,r}) + C_{b,r} \end{aligned} \tag{20}$$

- Body dynamics active.

$$\begin{aligned} \dot{x_1} &= \dot{x_2} \\ \dot{x_2} &= \frac{k_{c,f}v_f + k_{c,r}v_r}{k_{c,f}+k_{c,r}} \\ \dot{x_3} &= \dot{x_2} \\ F_f &= k_{c,f}(x_1 - p_f - L_{c,f} - \delta_f) \\ F_r &= -k_{c,r}(p_r - x_3 - L_{c,r} - \delta_r) \end{aligned} \tag{21}$$

2.4 Control Laws for Initial Parametric Study

For the initial study, we chose to implement the control approach developed by Sheikholeslam and Desoer. This control strategy is based on the exact linearization method to linearize and normalizes the input-output behavior of each vehicle in the platoon [17, 18, 19, 20, 21]. Using linearizing state feedback, they suggested the following control laws.

$$c_1 = c_{p1}\Delta_1(t) + c_{v1}\dot{\Delta}_1 + c_{a1}\ddot{\Delta}_1(t) + k_{v1}(v_l(t) - v_0) + k_{a1}a_l(t) \tag{22}$$

$$c_i = c_p\Delta_i(t) + c_v\dot{\Delta}_i + c_a\ddot{\Delta}_i(t) + k_v(v_l(t) - v_i(t)) + k_a(a_l(t) - a_i(t)) \tag{23}$$

where $c_{p1}, c_{v1}, c_{a1}, k_{v1}, k_{a1}, c_p, c_v, c_a, k_v$ and k_a are design parameters.

2.5 Case Studies : Simulation with MATLAB SIMULINK

The simulation code is written using SIMULINK in MATLAB. Figure 5 shows an overall SIMULINK diagram of a four-car platoon simulation *platoon* with an included collision dynamics module. The details inside the *lead, car* and *collision dynamics module* are shown in Figures 6, 7, and 8, respectively. Note that the inputs and outputs are connected to sequentially numbered input and output ports.

Figures 9-10 show the simulation results for a platoon control using feedback linearization with identical vehicles and nominal conditions. The input lead car velocity profile is given as a solid line in Figure 9(a). Nominal vaules for the parameters are 0.2 in τ_b, 0.2 in τ_e and 1.8 ($\times 10^3 kg$) in m_i where τ_b is the brake time constant, τ_e is the engine time constant and m_i is the i-th vehicle mass. We observe from these figures that the minimum spacings between each car can be controlled to the order of tens of centimeters. Since the spacing error approaches zero without oscillation as time increases, we see that string stability can be guranteed in nominal situations. These results give us a baseline nominal performance. To investigate the efffects of parametric variations on the platoon's behavior, the following simulations with randomly chosen parametric variations were performed.

CASE I :
The values of the perturbed parameters are given in the following tables. These varied

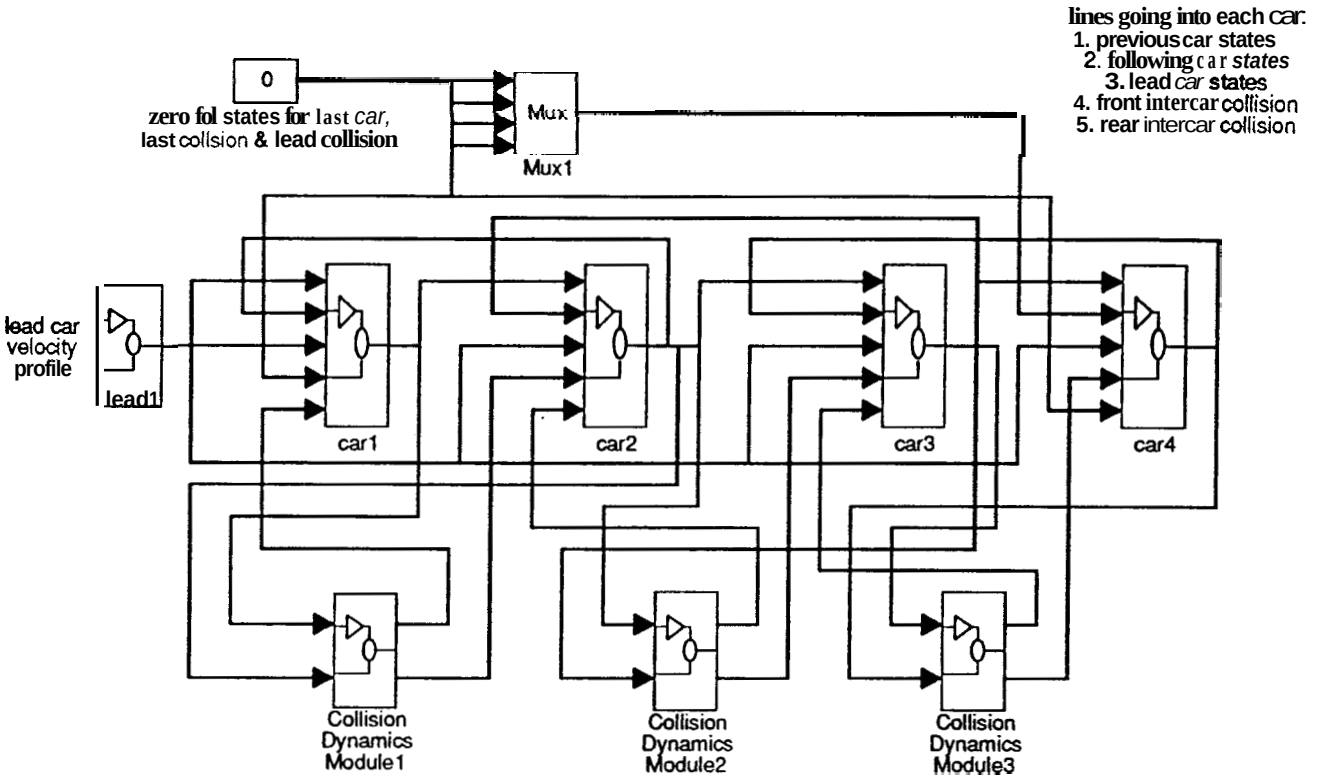

Figure 5: Overall Diagram of a Platoon Model

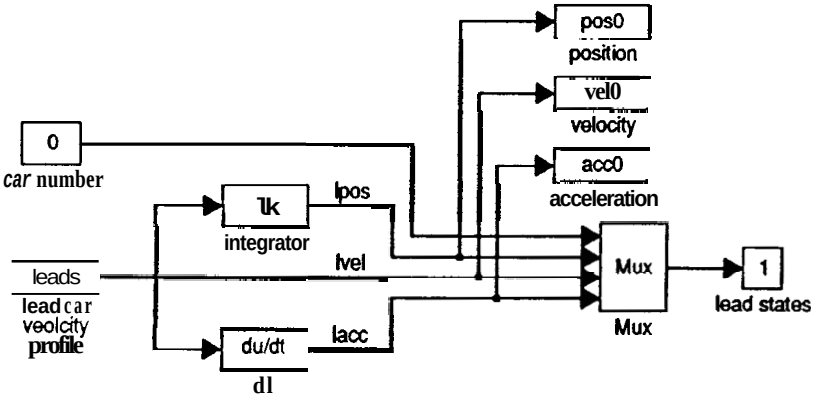

Figure 6: Inside Lead Module

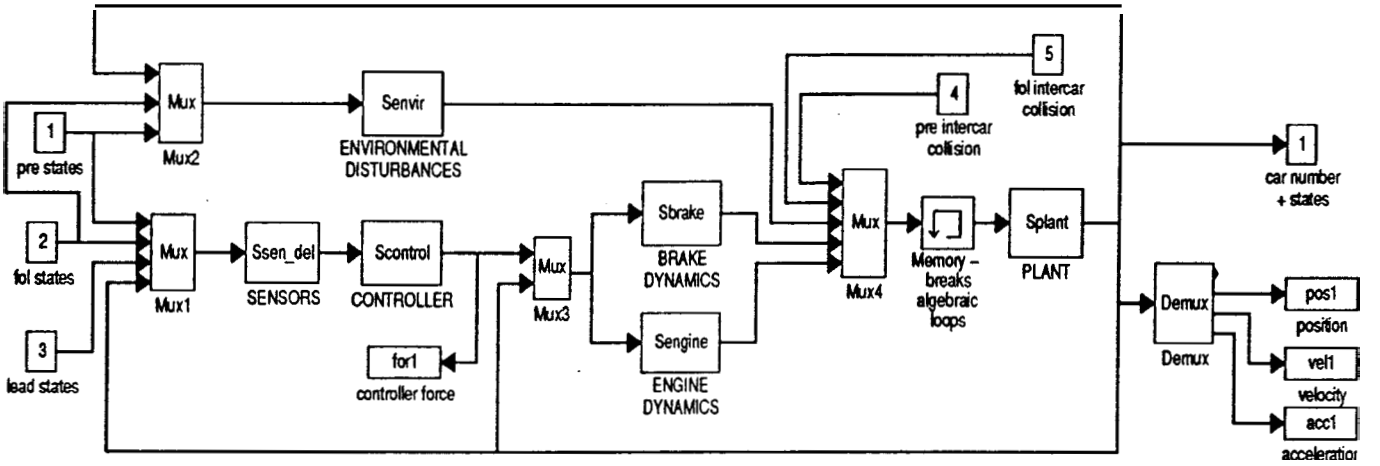

Figure 7: Inside Car Module

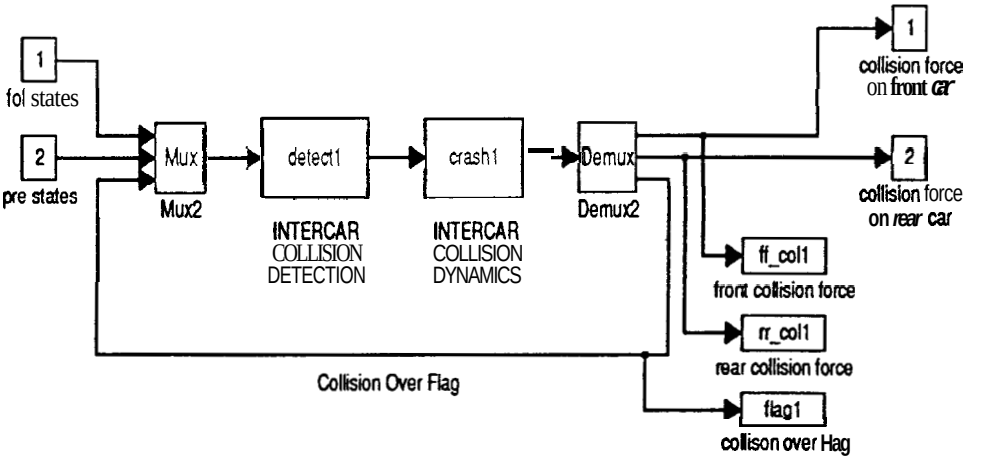

Figure **8:** Inside Collision Dynamics Module

parameters imply that the first and the third vehicles have good powertrain and braking systems while the second and the fourth have inferior systems. Figures 11 through **14** show the velocity/spacing responses, engine/brake forces, collision forces between each vehicle and the platoon length. From Figure 13, we see that the CDM is activated between car1 and car2 from **1.6** sec to 3.1 sec. When the intra-platoon collision occurred, the velocities of car1 and car2 match (Figure 11.a) and the spacing between these cars is zero (Figure 11.b).

Parameters	Car 1	Car 2	Car **3**	Car **4**
τ_b	0.1	0.3	0.1	0.3
τ_e	0.1	0.3	0.1	0.3
m_i	0.9	2.7	0.9	2.7

CASE II :

The following perturbed platoon was simulated in a manner similar to the previous case. The second and the fourth vehicles have better engine/brake systems than the first and the third. Figures **15-16** show the velocity, spacing and engine/brake responses. Although an intra-platoon collision did not occur (Figure 17), the platoon length increased (Figure 18).

Parameters	Car 1	Car 2	Car **3**	Car **4**
τ_b	**0.3**	0.1	0.3	**0.1**
τ_e	**0.3**	0.1	0.3	0.1
m_i	2.7	0.9	2.7	0.9

CASE III :

In this case, the first and the fourth vehicles have good brake/poor engine systems and the second and the third have poor brake/good engine systems. Figures 19-20 show the velocity, spacing and engine/brake responses. Figure **21** shows that the first collision occurred between car1 and car2, following which all cars in the platoon began to collide. Since an intra-platoon collision implies zero spacing, the platoon length **was** reduced, **as** seen in Figure **22.**

Parameters	Car 1	Car 2	Car 3	Car **4**
τ_b	0.1	0.3	0.3	**0.1**
τ_e	0.3	0.1	0.1	0.3
m_i	2.7	0.9	0.9	2.7

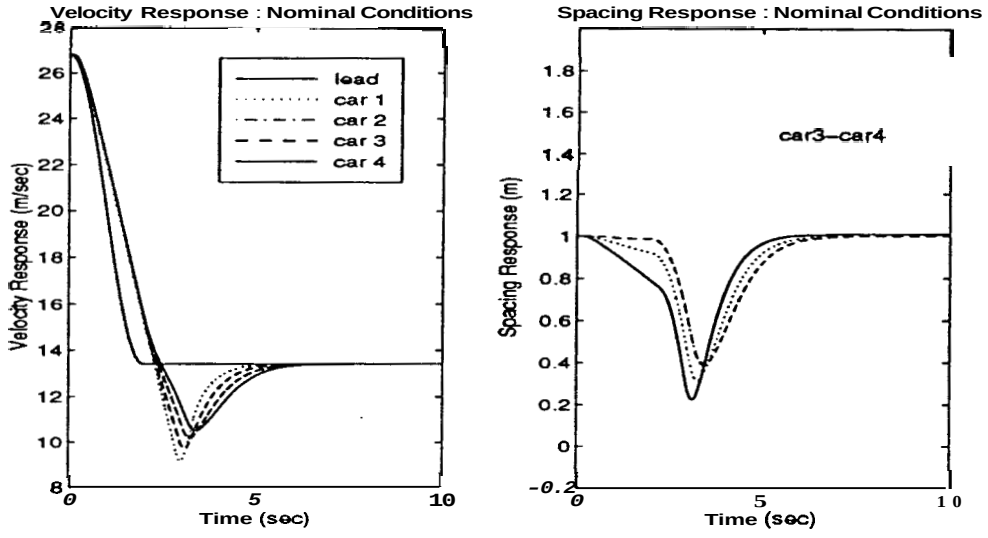

Figure **9:** Velocity and Spacing Responses with Nominal Conditions

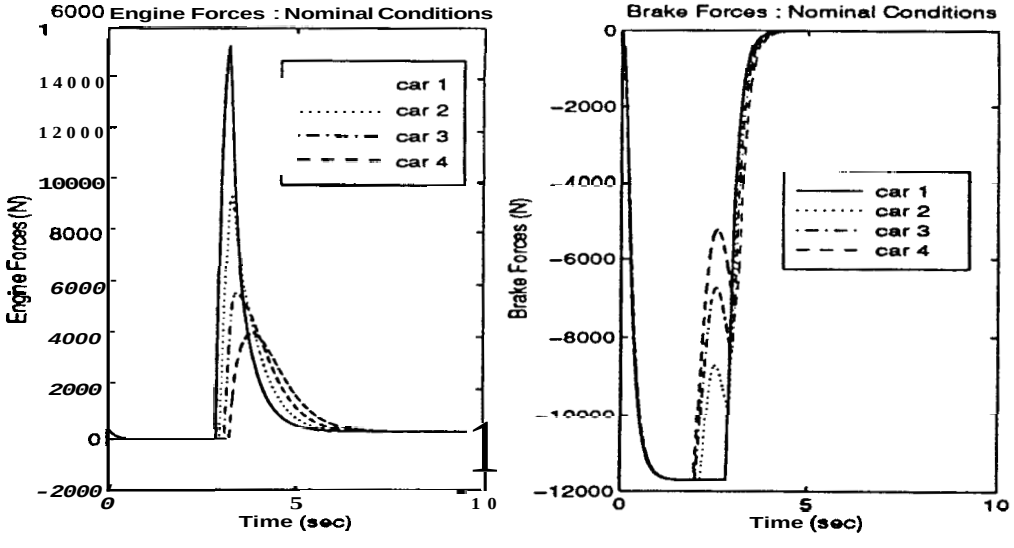

Figure 10: Engine and Brake Force Responses with Nominal Conditions

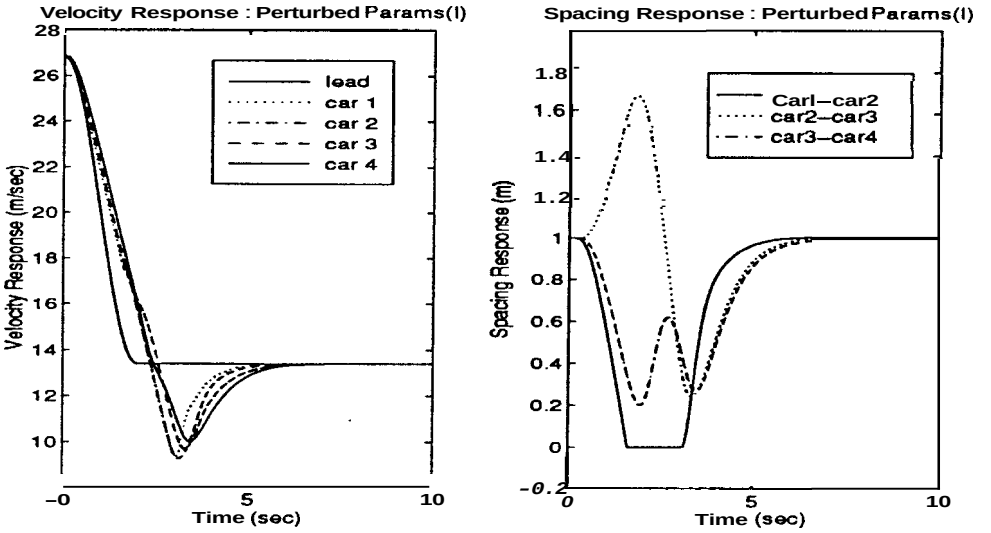

Figure 11: Velocity and Spacing Responses with perturbed Parameters : CASE(I)

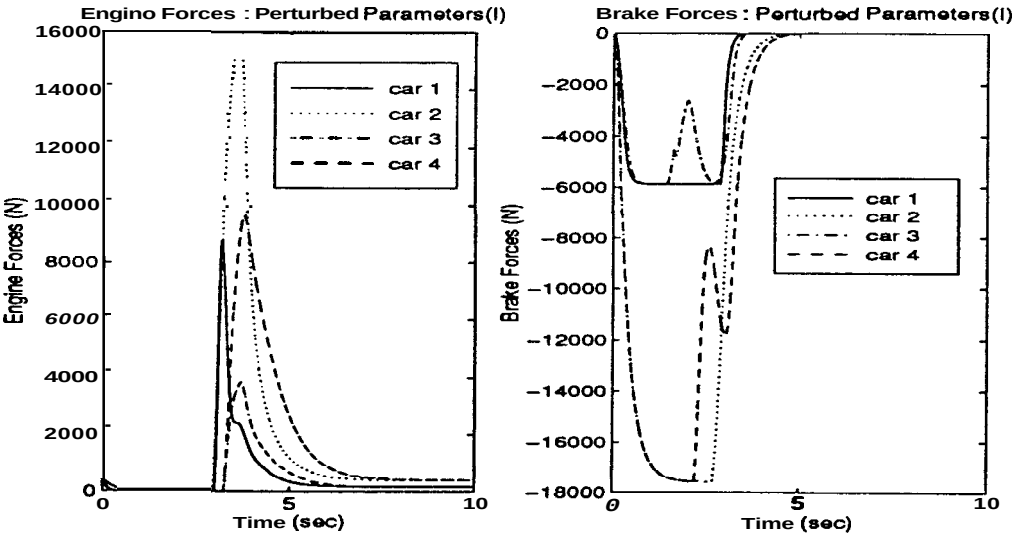

Figure 12: Engine and Brake Force Responses with Perturbed Parameters : CASE(I)

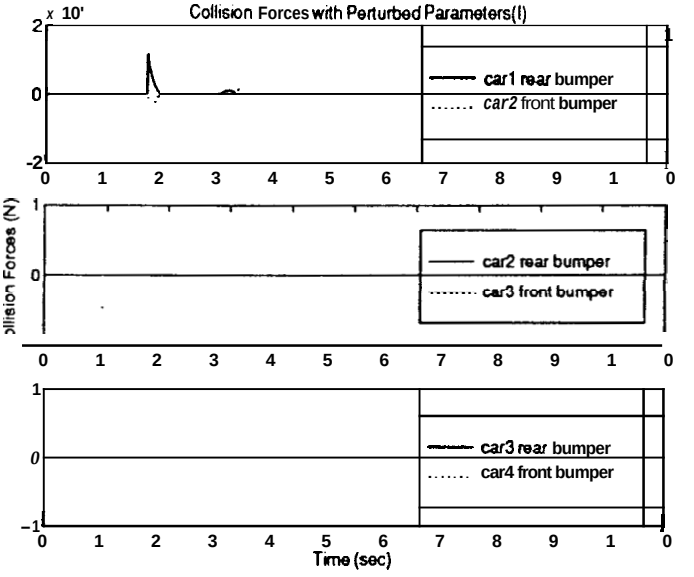

Figure **13:** Collision Forces with Perturbed Parameters : CASE(I)

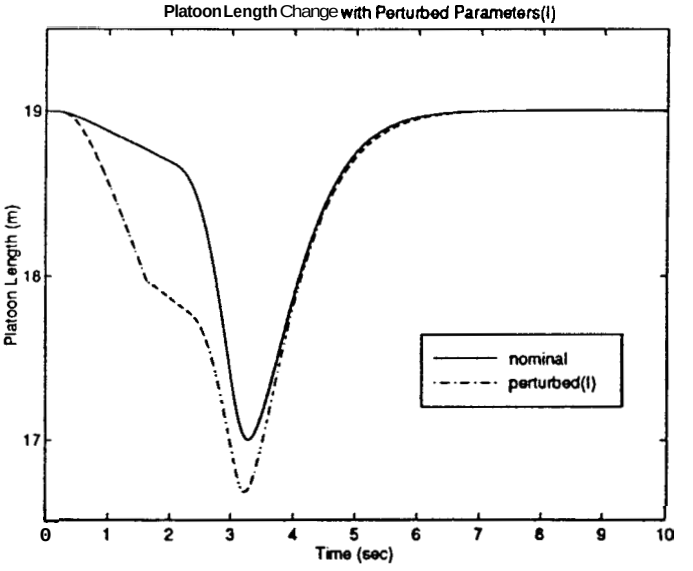

Figure **14:** Platoon Length with Perturbed Parameters : CASE(I)

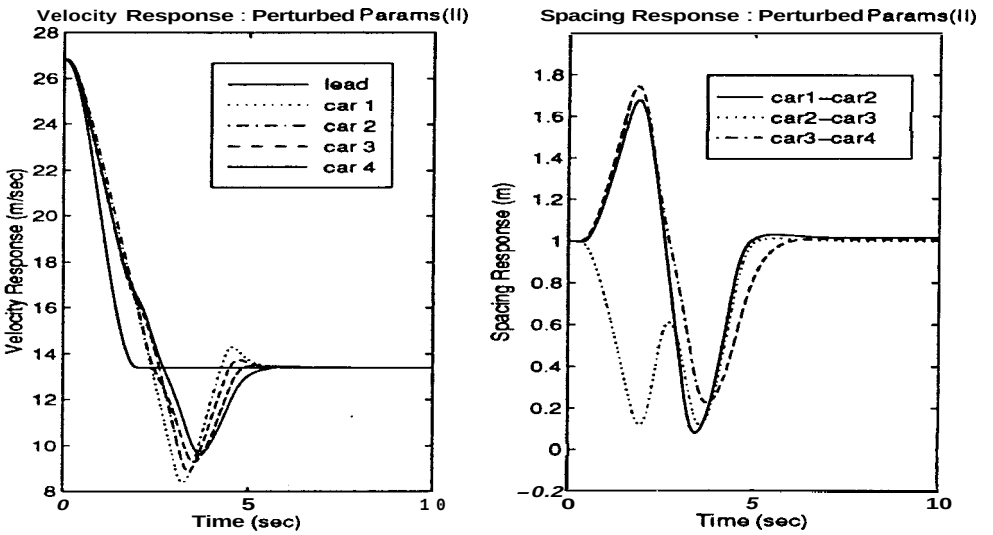

Figure 15: Velocity **and** Spacing Responses with Perturbed Parameters : CASE(II)

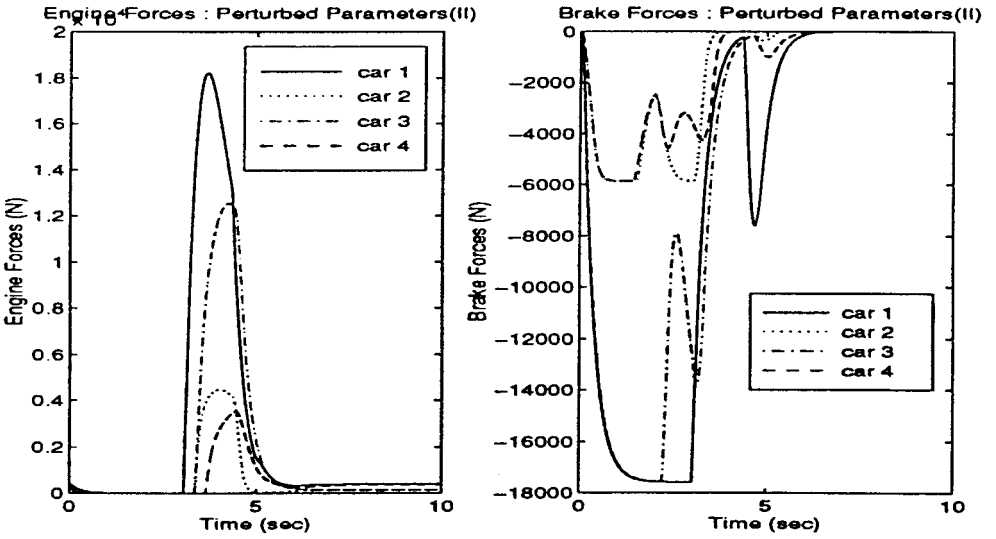

Figure 16: Engine and Brake Force Responses with Perturbed Parameters : CASE(II)

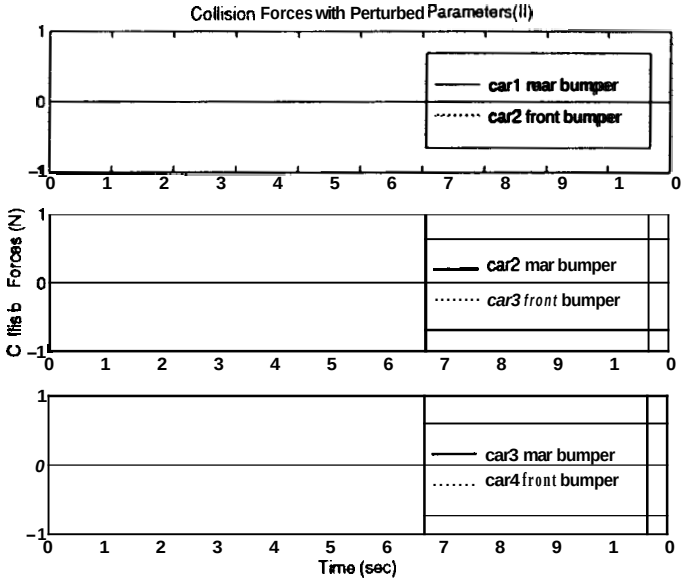

Figure 17: Collision Forces with Perturbed Parameters : CASE(II)

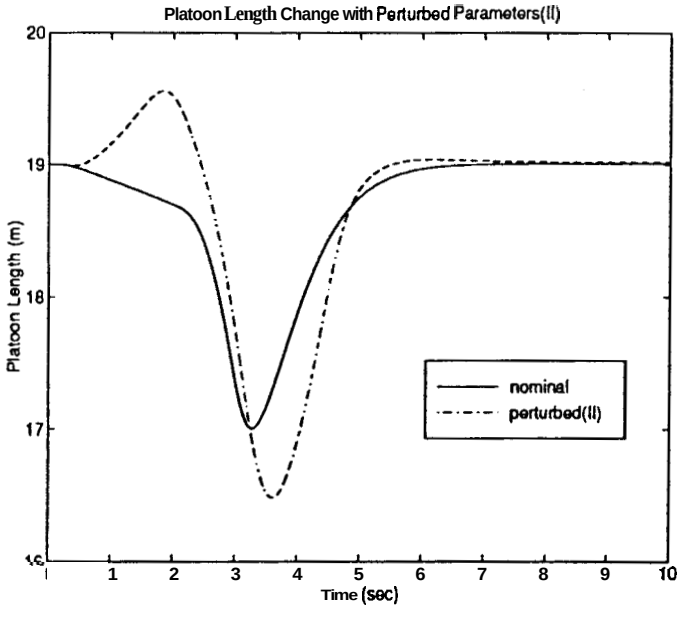

Figure **18:** Platoon Length with Perturbed Parameters : CASE(II)

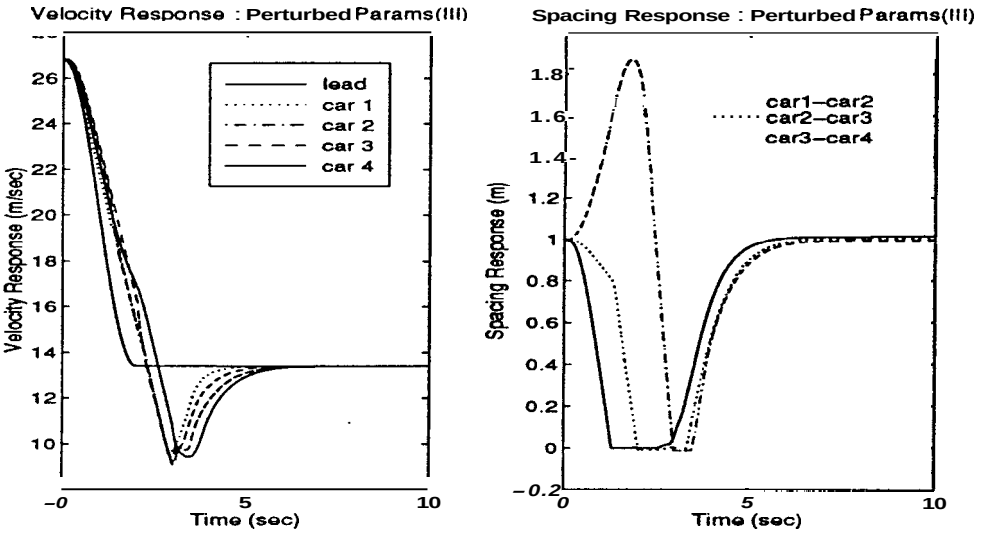

Figure 19: Velocity and Spacing Responses with Perturbed Parameters : CASE(III)

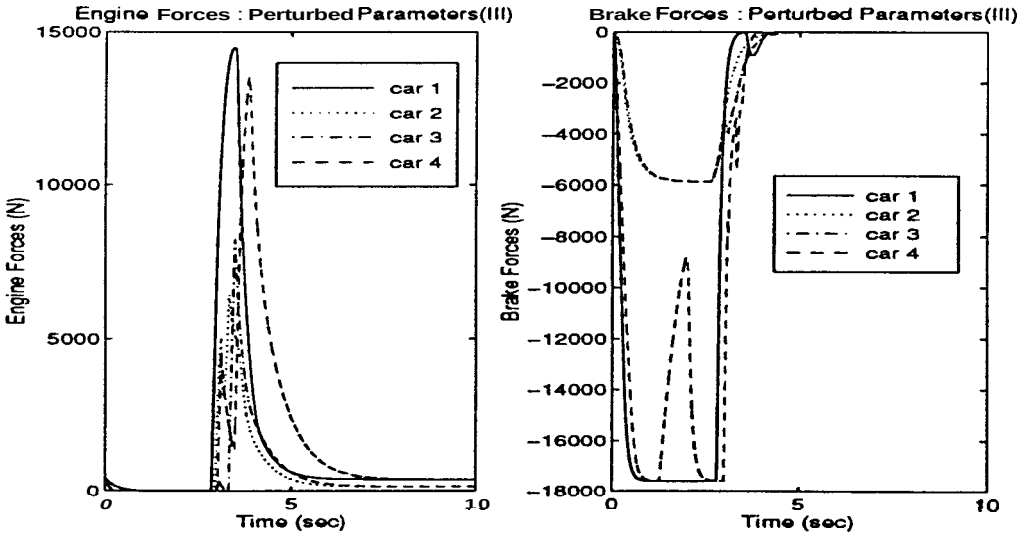

Figure **20:** Engine and Brake Force Responses with Perturbed Parameters : CASE(III)

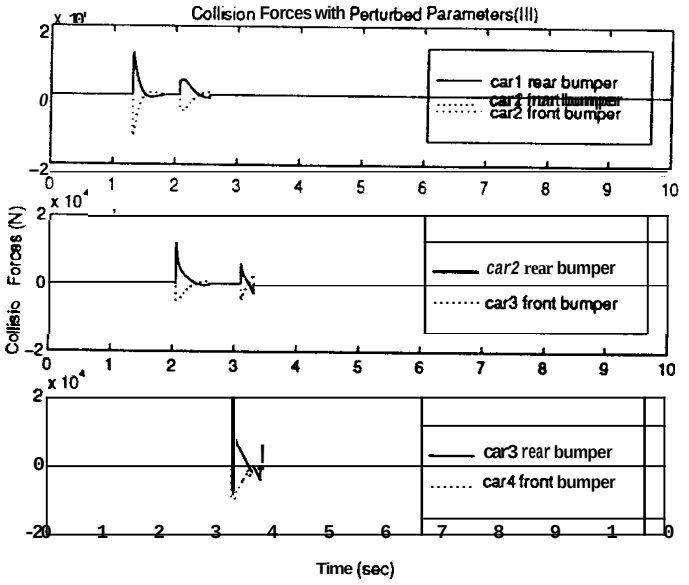

Figure **21:** Collision Forces with Perturbed Parameters : CASE(III)

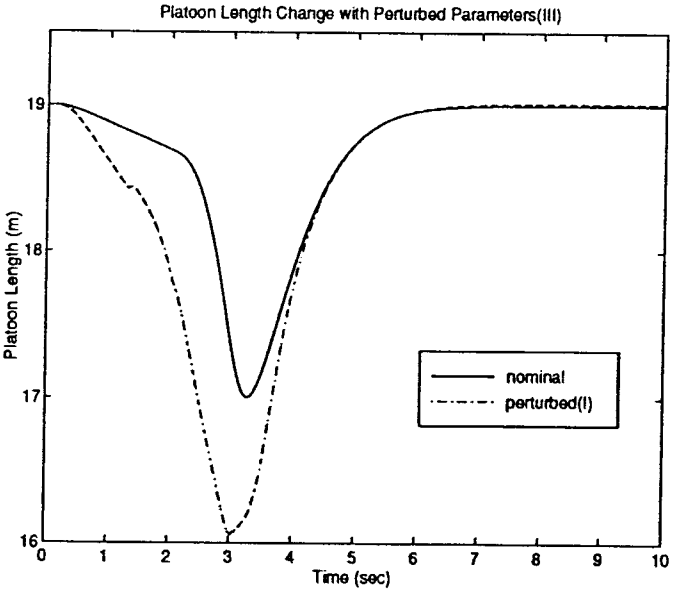

Figure 22: Platoon Length with Perturbed Parameters : CASE(III)

3 Effects of Vehicle Incompatibilities within Platoon

The Platoon Simulation Package (PSP) described in Section 2 has been used to study the effects of vehicular non-uniformity within a platoon. To examine the behavior of the platoon as a result of changes in vehicle parameters, simulations for a platoon consisting of four non-identical vehicles were performed under an emergency scenario. These effects are described below.

3.1 Brake Time Constant Variations

For this study, the effect of parametric variation is examined by altering the brake time constants from vehicle to vehicle. In order to investigate the effects of brake time constant variations upon platoon performance, we assumed that the second car had a worsened braking capacity. That is, the brake time constant in the second car was set to 0.3 while the other cars had a nominal value of 0.2. Simulation results are given in Figure 23. In this case, intra-platoon collision occurred between the first car and the second. It can be seen that the velocities of the first and second car are same during the collision period (2-3.2 sec). Also, it shows that the spacing between the first and second car is zero in this collision time region. This behavior matches our intuition since the second car had inferior brake performance, causing the second car to collide with the more quickly decelerating first car. Note that vehicles in this simulation were using the feedback linearization controller suggested by Sheikholeslam and Desoer [17]. A significant improvement in the platoon's behavior can be obtained using a robust H_∞ controller, the design of which is described in Section 4.

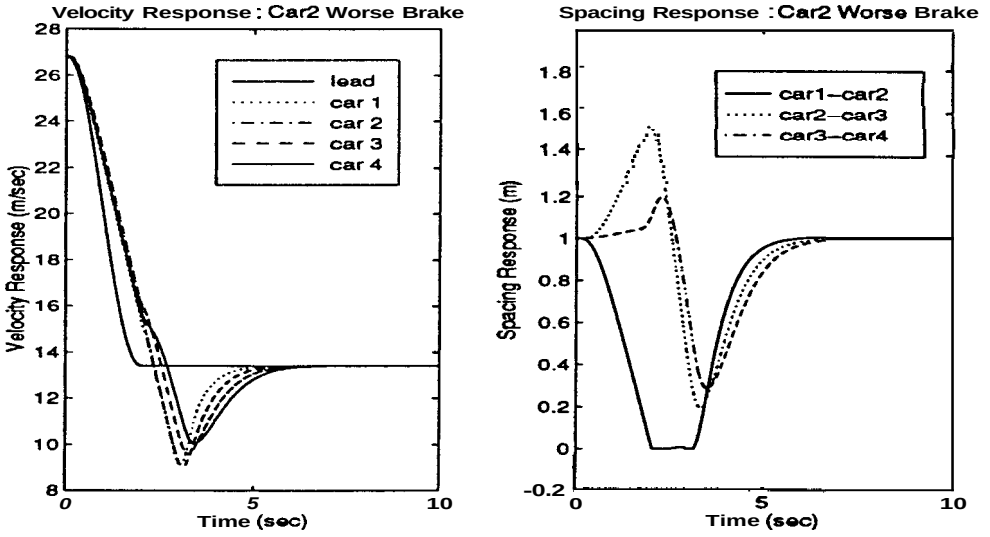

Figure 23: Velocity and Spacing Responses when Car2 has Worse Brake

The significance of brake systems to the performance of platoon control is explained here. We assumed that the brake time constant has the value 0.2 with ± 50% uncertainty to see the effects of the varying brake time constants. For a four car platoon, we set the perturbed value of brake time constant in one vehicle and nominal values in others. The simulation results are illustrated in Section **3.2.**

3.2 Vehicle Ordering in Platoon

To determine the vehicle ordering in a platoon such that platoon *can* be stopped without any collisions (dead-stop condition) and platoon length is minimized (high density), intra-platoon collisions, maximum platoon length, intra-platoon minimum spacing and accident collision indices are considered. Simulations are carried out by varying the vehicle brake constant distributions (0.1-0.3), the results of which are described below.

Remark : We assumed that each car's deceleration can be directly manipulated up to a maximum value and all vehicle data are immediately available.

• Intra-platoon Collision :
Intra-platoon collisions are investigated when one of vehicles in platoon **has** a perturbed brake time constant. '*' and 'o' indicates a collision and no collision respectively in Figure 24. Collisions occurred when the first car has good brakes (τ_b=0.1, 0.12), the second has relatively worse brakes (τ_b=0.26-0.3) and the third has the worst brake systems (τ_b=0.3). In Figure **24,** the text column of each collision case shows the time when collision occurred and which cars collided. Most collisons occurred between the first and second cars except car2-car3 collision when the third car has the worst brake time constant (τ_b=0.3). Figure 25 shows the maximum platoon length.

• Intra-platoon Minimum Spacing :
Figure 26 shows the minimum intra-platoon spacing when a platoon includes a car with perturbed brake time constant. In this figure, 'x' indicates that car2-car3 has minimum spacing and 'o' indicates that car3-car4 has minimum spacing. The other cases have minimum spacing between car1 and car2. Note that intra-platoon minimum spacing during a maneuver relates to the level of highway congestion and the relative probability of a collision. The consideration of intra-platoon minimum spacing is **aimed** at achieving an effective trade-off between the two objectives, highway congestion and safety when designing the platoon longitudinal controller.

• **Accident Collision Index :**
In order for a meaningful analysis to be performed with respect to the potential for injury

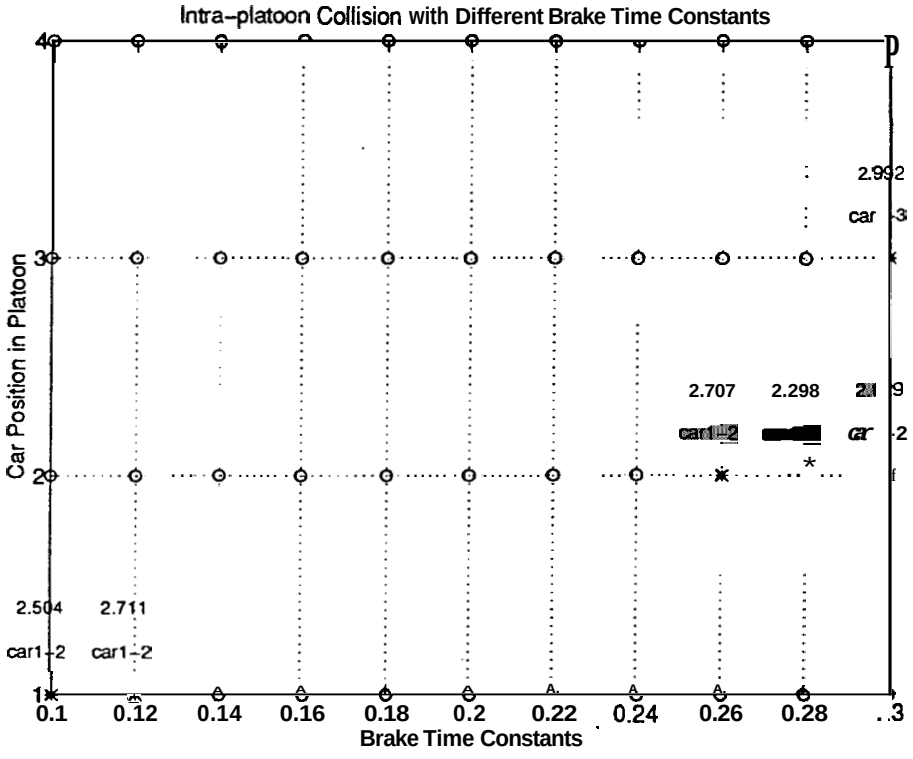

Figure **24:** Intra-platoon Collisions within Platoon : Varying the Position of Vehicle Having Perturbed Brake Time Constant

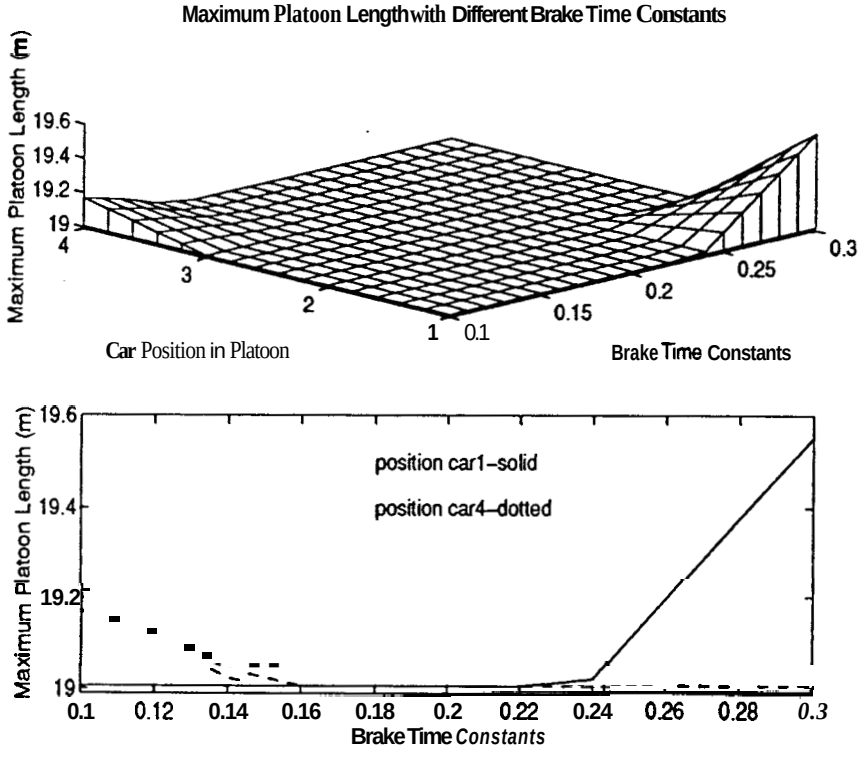

Figure **25:** Maximum Platoon Length

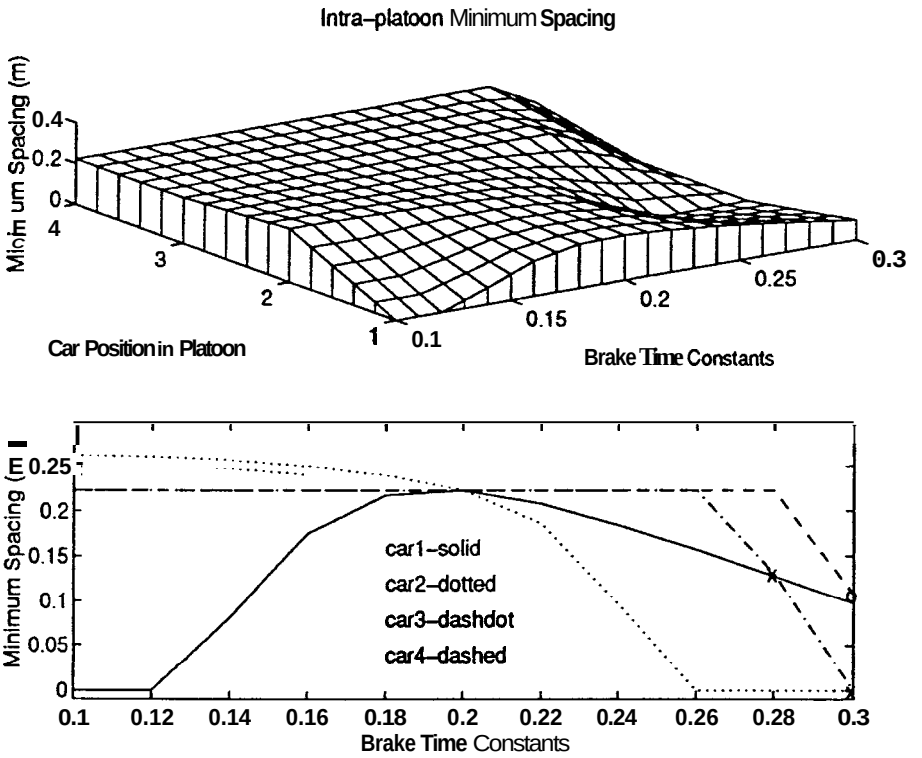

Figure 26: Minimum Spacing

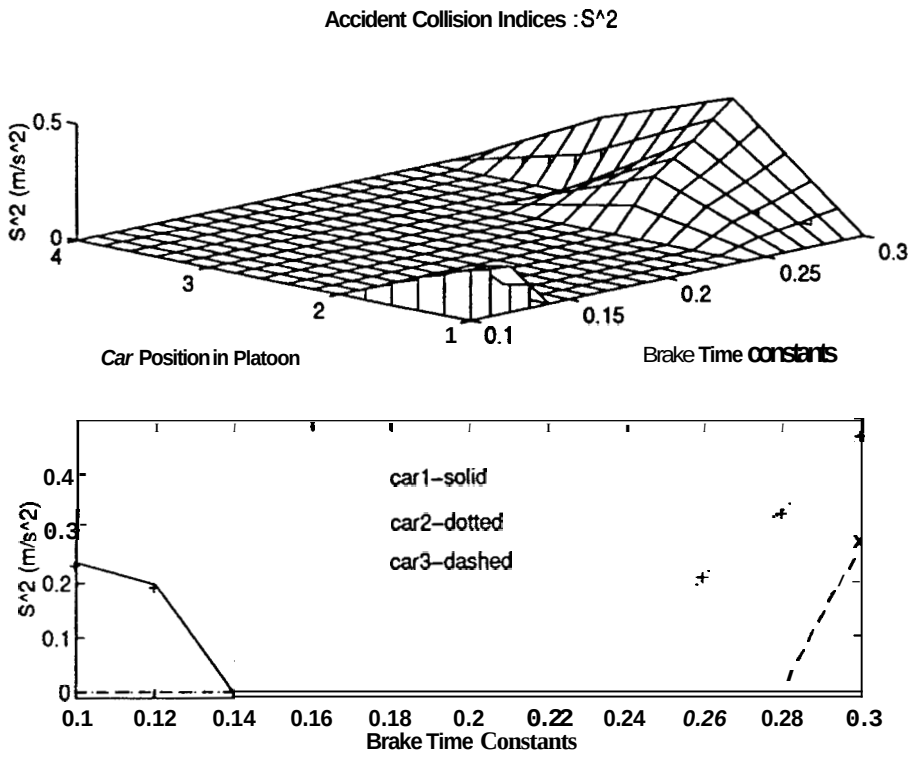

Figure 27: Accident Collision Indices : S^2

during a collision, some indication of collision severity is necessary. To quantify the severity of collision, Glimm and Fenton introduced the Accident Severity Index(S^2) which is defined by [6]

$$S^2 = [\Delta \dot{x}(t_c)]^2 = [\dot{x}_l(t_c) - \dot{x}_t(t_c)]^2 \tag{24}$$

where t_c denotes the time when collision occurred, $\Delta \dot{x}(t_c)$ denotes the relative collision velocity and $\dot{x}_l(t_c)$, $\dot{x}_t(t_c)$ denote the leading car velocity and the trailing car velocity at t_c, respectively. Figure 27 shows the Accident Severity Indices when a platoon includes a vehicle with a varied brake parameter.

The following can be observed from the results shown in Figures 24-27. The platoon length is minimized when the car braking capabilities are ordered from the weakest to strongest and the dead-stop distance of the overall platoon matches that of the weakest decelerating car. The dead-stop distance is minimized when the cars are ordered from the strongest braking to the weakest, which produces a dead-stop distance equal to that of the strongest car. This ordering approach also produces a relatively long platoon. The shortest platoon produces the longest dead stop performance (ordering-worst braking to best) and the longest platoon

allows the shortest dead stop performance (ordering-best braking to worst),

How do observations like these help the designer? If platoons are to be formed from non-uniform vehicles, as would seem likely, it becomes the task of the platoon's designer to optimize the platoon in the face of these non-uniformities. One must, of course, balance different needs and requirements. For the case just discussed, that of dead stop behavior, it is seen that ordering the vehicles so that the strongest braking occurs at the front allows the most rapid stops and thus an enhanced margin of operational safety. Clearly, this is something that a hierarchical controller would need to ensure if safety was weighted strongly in the performance mix. The performance level of a vehicle (braking, acceleration, etc.) would need to be transmitted to the upper level controller which could then order the vehicles according to a predetermined optimality condition (shortest stop time, shortest platoon, etc.).

4 H_∞ Longitudinal Controller

4.1 Problem Statements and Objectives

The simulations in Section 3 were run using the feedback linearization controller suggested by Sheikholeslam and Desoer [17]. Although their feedback linearization controller guarantees string stability of platoon under nominal conditions, parametric uncertainties are not considered in the control design. To address this problem, we designed a new dynamic controller based on H_∞ theory. This approach is essentially a frequency domain optimization method for designing robust control systems. The main concern is to provide robustness with respect to parameter variations and reasonable performance with respect to exogenous inputs.

Section 4.2 gives a detailed explanation of the linearized vehicle model. Section 4.3 gives the representation of this model as an interconnection structure. The controller design is presented in Section 4.4-4.5 and simulations are presented in Section 4.6.

4.2 Linearized Vehicle Model

A linearized model of an vehicle can be obtained by performing a small perturbation on all vehicle variables. The equation of vehicle motion is of the form

$$\mathbf{f}(\dot{\mathbf{x}}, \mathbf{x}, \mathbf{u}, \mathbf{y}) = 0 \tag{25}$$

where $\mathbf{x}$ is a vector of state variables (position, velocity and a powertrain state); $\mathbf{u}$ is the vector of inputs (wind gusts, road slope and powertrain input); and $\mathbf{y}$ is the vector of desired outputs, such as desired position, velocity and acceleration. When a small displacement, denoted by δ, is applied to each of the components of the $\mathbf{x}$, $\mathbf{u}$, and $\mathbf{y}$ vectors, the perturbed variables will still satisfy the governing equations] i.e.

$$\mathbf{f}(\dot{\mathbf{x}}_0 + \delta\dot{\mathbf{x}}, \mathbf{x}_0 + \delta\mathbf{x}, \mathbf{u}_0 + \delta\mathbf{u}, \mathbf{y}_0 + \delta\mathbf{y}) = 0 \tag{26}$$

where the subscript, $_0$, denotes the steady-state value before disturbance. In steady-state, $\dot{\mathbf{x}}_0 = 0$ and

$$\mathbf{f}(\mathbf{x}_0, \mathbf{u}_0, \mathbf{Y}_0) = 0 \tag{27}$$

The above steady-state relations can be back-substituted into Equation (26) to simplify it. When higher order δ terms are ignored, the remaining terms can be regrouped and written in the following standard state space form

$$\delta\dot{\mathbf{x}} = \mathbf{A}\delta\mathbf{x} + \mathbf{B}\delta\mathbf{u} \tag{28}$$

$$\delta\mathbf{y} = \mathbf{C}\delta\mathbf{x} + \mathbf{D}\delta\mathbf{u} \tag{29}$$

With MATLAB/SIMULINK, the whole perturbation and regrouping process of determing the values of the $[\mathbf{A},\mathbf{B},\mathbf{C},\mathbf{D}]$ matrices of a nonlinear vehicle system can be done numerically, i.e. the procedure to obtain the numerical values of the $[\mathbf{A},\mathbf{B},\mathbf{C},\mathbf{D}]$ matrices about some desired operating point can be accomplished through the following steps.

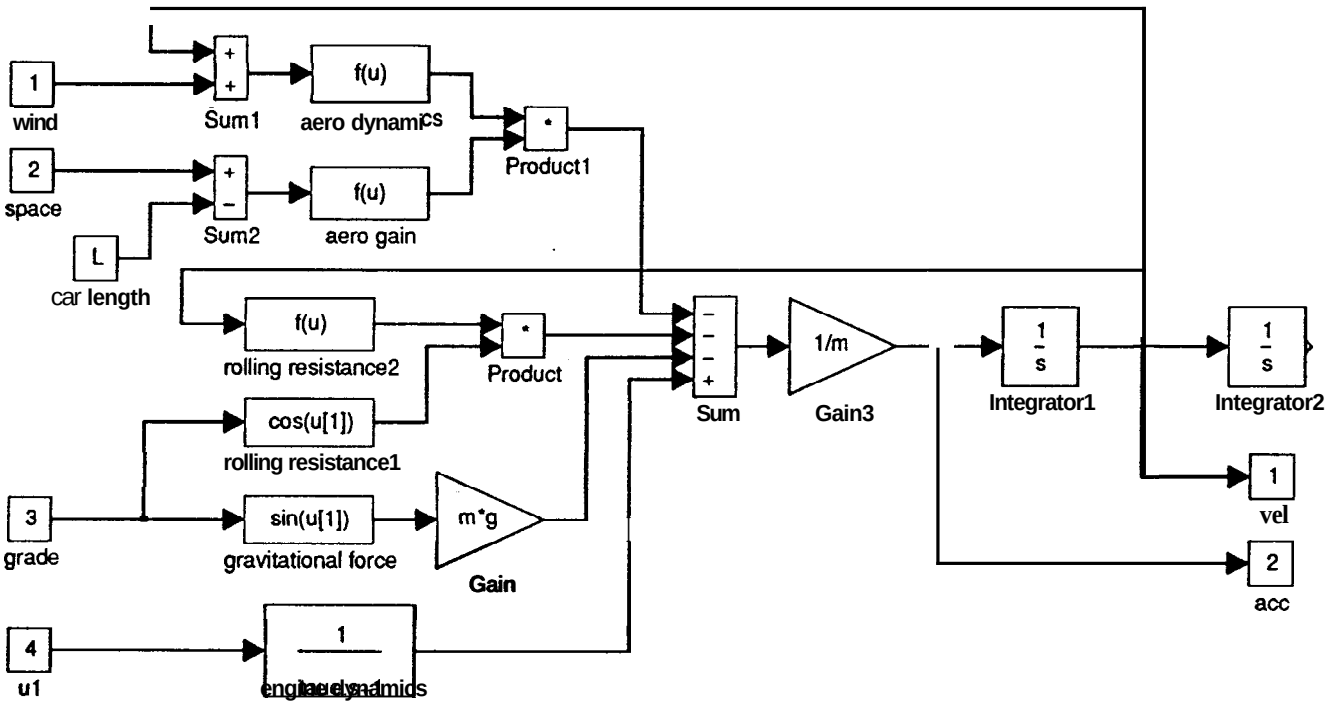

Figure 28: Overall Diagram of ***vehicle***

The complete steady-state of the SIMULINK system at some desired operating point must be determined using the SIMULINK **trim** function,

$$[\mathbf{x_0},\mathbf{u_0},\mathbf{y_0}] = trim['vehicle',\mathbf{x_0^g},\mathbf{u_0^g},\mathbf{y_0^g}] \tag{30}$$

In the preceding equation ***vehicle*** is the filename of the SIMULINK simuation of the system with all its inputs **u** defined by input ports numbered in the same sequence as in **u,** all its outputs **y** defined by output ports numbered in the same sequence as in **y,** and **x** the vector of the state variables. The actual ordering of the states in **x** by SIMULINK can be determined using the **MATLAB** function,

$$[sizes,\mathbf{x_0},xstr] = vehicle([\,],[\,],[\,],0) \tag{31}$$

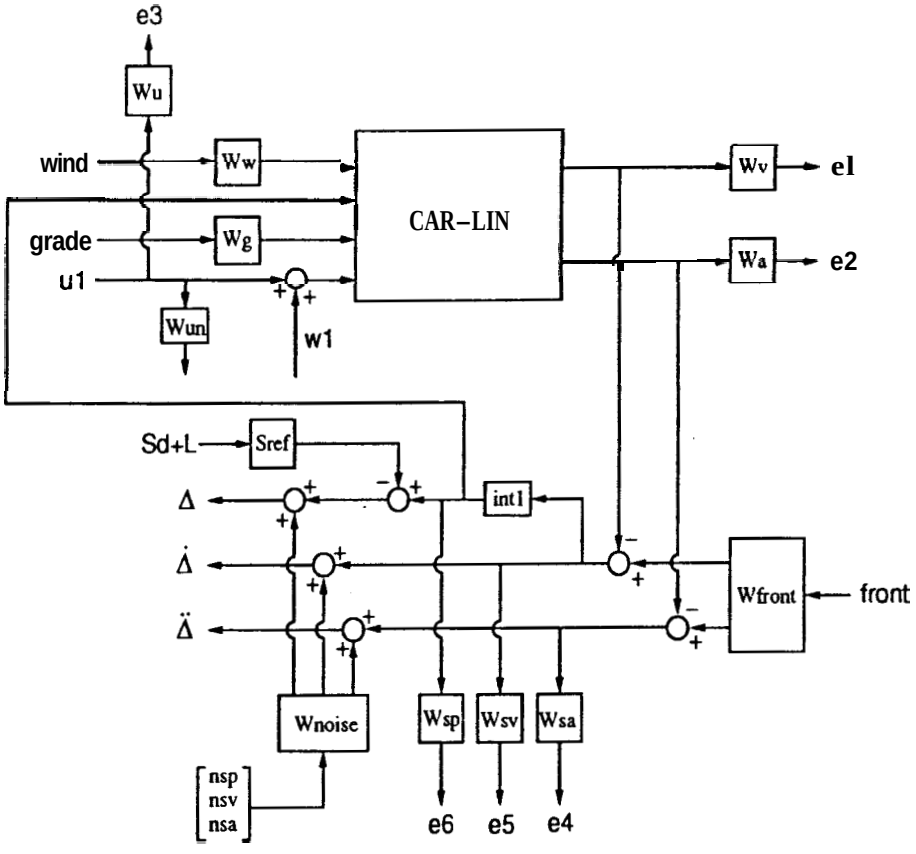

Figure 29: Interconnection Structure of a Vehicle in Platoon, *car_ic*

The **trim** function uses a quadratic nonlinear programming algorithm. Good initial guesses of $\mathbf{x}_0, \mathbf{u}_0$ and $\mathbf{y}_0$ are to be provided to the function through $\mathbf{x}_0^g, \mathbf{u}_0^g$ and $\mathbf{y}_0^g$. Index variables can be used to specify which elements of $\mathbf{x}_0, \mathbf{u}_0$ and $\mathbf{y}_0$ are to be held fixed and which are allowed to change during the iterations for the steady-state. When the initial values are obtained, we can proceed to use the MATLAB **linmod** function to determine the $[\mathbf{A},\mathbf{B},\mathbf{C},\mathbf{D}]$ matrices of the small signal model of the nonlinear system about the chosen steady-state operating point. Figure 28 shows an overall diagram of the simulation ***vehicle.*** Note that the inputs and outputs are connected to sequentially numbered input and output ports **as** required by **trim** and **linmod** to obtain the steady-state and small signal model.

4.3 Open-Loop Interconnection

The open-loop interconnection structure, which includes the uncertainties and the performance objectives, is shown in Figure **29.** The linearized vehicle model (*CAR_LIN*) is obtained **as** discussed in the previous section. The weighting functions are chosen by considering input

and output units. In the Matlab workspace, the open-loop system is denoted by *car-ic*, and has 7 states, 10 outputs and **9** inputs. **A** schematic diagram, with the specific input/output ordering for *car-ic*, is shown in Figure **30,** followed by explanation of variable contents.

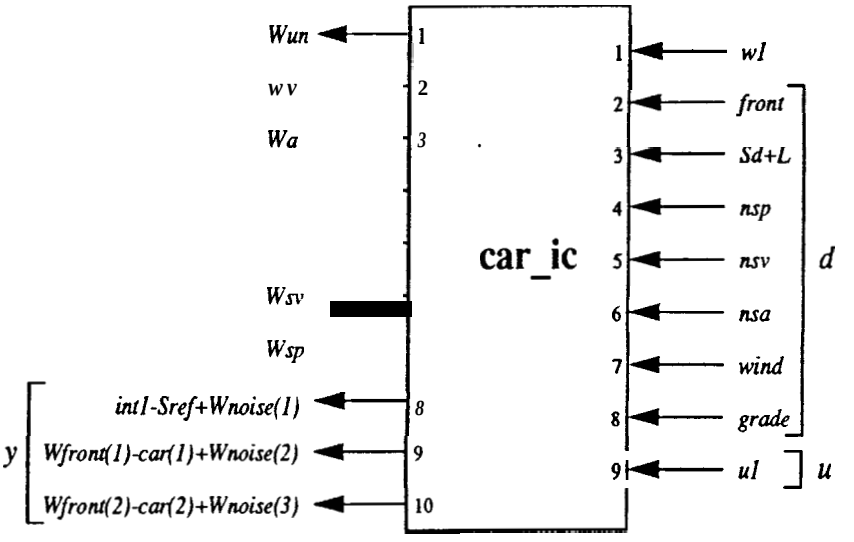

Figure **30:** Schematic Diagram of a Vehicle in Platoon, *car-ic*

10 outputs	**9** Inputs
W_{un} = perturbed output (uncertainty)	**wl** = perturbed input (uncertainty)
W_v = weighted velocity of current car	$front$ = previous car input
W_a = weighted acceleration of current car	$S_d + L$ = desired spacing + vehicle length
W_{u1} = weighted control input	nsp = sensor noises of S
W_{sa} = weighted $\ddot{S}$	nsv = sensor noises of S
W_{sv} = weighted $\dot{S}$	nsa = Sensor noises of S
W_{sp} = weighted S (S:=spacing)	***wind*** = wind gusts
$\Delta = int1 - S_{ref} + W_{noise}(1)$	***grade*** = road slope
$\dot{\Delta} = W_{front}(1) - car(1) + W_{noise}(2)$	$u1$ = control input
$\ddot{\Delta} = W_{front}(2) - car(2) + W_{noise}(3)$	

4.4 Uncertainty Model

The control input is weighted to represent model uncertainty. Given this nominal model *CAR_LIN* (i.e., $G_{nom}(s)$) we also specify a stable 1×1 transfer matrix $W_{un}(s)$, called the uncertainty weight. These two transfer matrices parametrize an entire set of plants, $\mathcal{G}$, which must be suitably controlled by the robust controller K.

$$\mathcal{G} := \{G_{nom}(I + \Delta_G W_{un}) : \Delta_G \text{ stable}, \|\Delta_G\|_\infty \leq 1\}$$

All of the uncertainty in modeling the vehicle is captured in the normalized, unknown transfer function Δ_G. The unknown transfer function Δ_G is used to parameterize the potential differences between the nominal model $G_{nom}(s)$, and the actual behavior of the real vehicle, denoted by G. The dependence on frequency of the uncertainty weight indicates that the level of uncertainty in the vehicle's behavior depends on frequency.

The uncertainty weight is of the form $W_{un}(s) := w_{un}(s)I$, where I is an identity matrix, for a given scalar valued function $w_{un}(s)$. The fact that the uncertainty weight is diagonal, with equal diagonal entries, indicates that the modeled uncertainty is in some sense a "round ball" about the nominal model G_{nom}. The weight chosen for this problem is $w_{un} = \frac{5s+1.02}{s+10.2}$. The set of plants that are represented by this uncertainty is:

$$\mathcal{G} := \{G_{nom}(I + \frac{5s + 1.02}{s + 10.2}\Delta_G(s)) : \Delta_G \text{ stable}, \|\Delta_G\|_\infty \leq 1\}$$

A frequency response of w_{un} is shown in Figure 31.

4.5 Controller Design

The controller receives three sensor measurements: $\Delta(t)$, $\dot{\Delta}(t)$ and $\ddot{\Delta}(t)$. $\Delta(t)$ denotes the spacing error, i.e. $\Delta(t) = S(t) - S_d$ where $S(t)$ is the spacing between the previous car and current car, and S_d is the desired spacing, which is set to 1m in this report. The controller produces one output signal for the control force command. The controller block diagram is shown below.

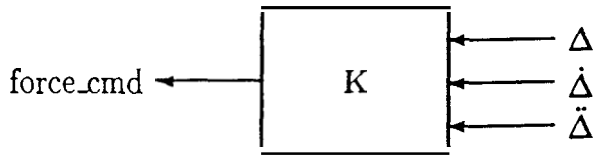

In this section the robustness properties of two different controllers are analyzed using μ. Each controller has different characteristics:

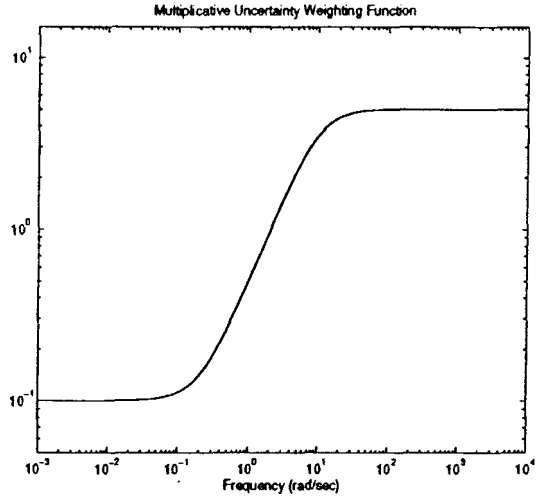

Figure **31:** Multiplicative Uncertainty Weighting Function

- k_h is designed to optimize H_∞ performance, under the assumption of no model uncertainty
- ***k-mu*** is designed with the $D-K$ iteration approach to μ-sysnthesis

H_∞ Design on the Open-loop Interconnection

Note that the first step to the $D-K$ interation is an H_∞ (sub)optimal control design for the open connection, ***car-ic.*** In terms of iteration, this amounts to holding d variable fixed (at **1),** and minimizing the $\|\cdot\|_\infty$ norm of $F_L(P,K)$, over the controller variable K. $F_L(P,K)$ is the nominal closed loop transfer function from the perturbation inputs and the disturbances to the perturbation outputs and errors (z and ***e),*** which are shown below. The function hinfsyn in MATLAB p-tools designs **a** (sub)optimal H_∞ control law based on the open-loop interconnection structure provided to it.

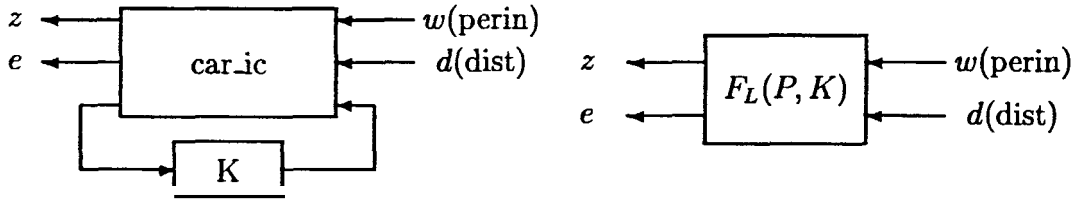

D-K Iteration

The p-tool **dkit** automates the p-synthesis procedure via $D-K$ interation. The iteration summary is given in below table and Figure **32** shows the corresponding μ plots for controller #1 and #2, respectively.

Iteration Summary

iteration #	1	2	3	4
Controller Order	7	9	11	11
Total D-Scale Order	0	2	4	4
Gamma Achieved	10.093	1.492	1.395	1.366
Peak μ-Value	2.679	1.492	1.369	1.369

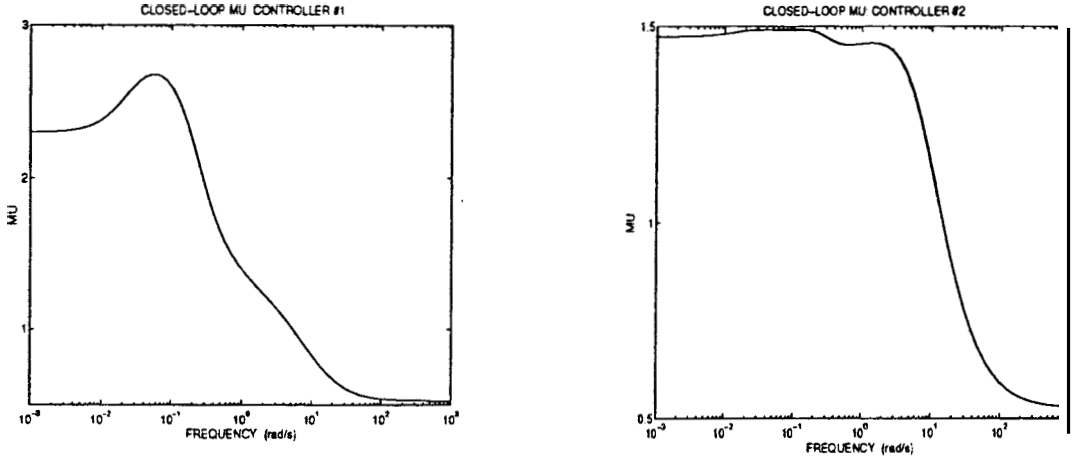

Figure 32: μ Plots for Controllers, #1 and #2

4.5.1 Nominal Frequency Response

The closed-loop system is constructed using the star product (Figure **33).** In the closed-loop system, there are seven exogeneous signals and ***six*** errors. The nominal performance objective is that this multi-variable transfer function matrix should have an H_∞ norm less than **1.**

Since ***k_h*** was designed specially with disturbances and errors in mind, the better nominal performance is achieved by controller ***k_h*** and the performance from ***k-mu*** is relatively poor **as** seen in Figure **34.** It comes from that the degradation of ***k_mu*** nominal performance is offset by much greater insensitivity to variations.

The peak norms of the closed-loop system are calculated for each input/output channel with both controllers.

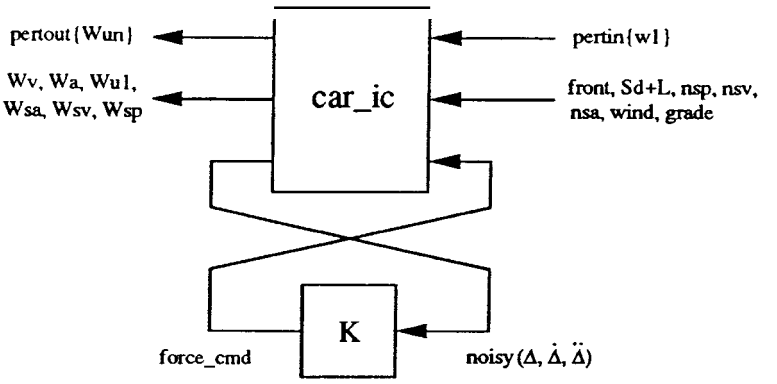

Figure **33:** Star Product

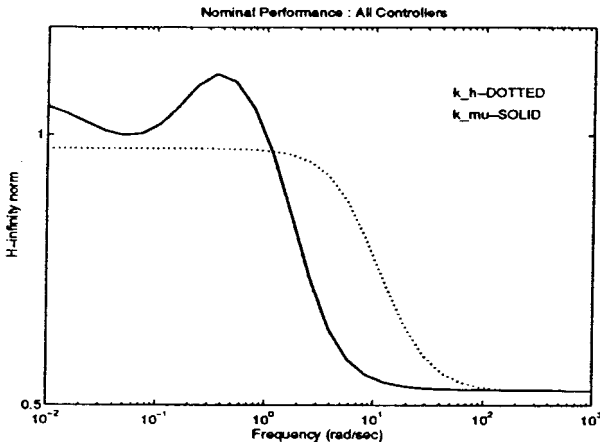

Figure **34:** Nominal Performance of k_h(dotted) and k_mu(solid)

k_h

	$front$	$S_d + L$	nsp	nsv	nsa	$wind$	$grade$
Wv	0.6068	0.0273	0.0005	0.0326	0.0815	0.0427	0.1839
Wa	0.8257	0.0291	0.0006	0.0191	0.1530	0.1224	0.5270
$Wu1$	0.5856	0.1111	0.0022	0.1328	0.2043	0.1226	0.5277
Wsa	0.0205	0.0003	0.0000	0.0002	0.0015	0.0012	0.0053
Wsv	0.0186	0.0009	0.0000	0.0011	0.0027	0.0014	0.0061
Wsp	0.0409	0.0091	0.0002	0.0109	0.0167	0.0085	0.0367

k_mu

	$front$	$S_d + L$	nsp	nsv	nsa	$wind$	$grade$
Wv	0.6212	0.0261	0.0005	0.0290	0.1800	0.0350	0.1507
Wa	0.8004	0.0231	0.0005	0.0181	0.2922	0.1197	0.5155
$Wu1$	0.6366	0.1064	0.0021	0.1181	0.4324	0.1075	0.4628
Wsa	0.0200	0.0002	0.0000	0.0002	0.0029	0.0012	0.0052
Wsv	0.0210	0.0009	0.0000	0.0010	0.0060	0.0012	0.0050
Wsp	0.0438	0.0087	0.0002	0.0097	0.0354	0.0073	0.0315

4.5.2 Robust Stability and Robust Performance

In this section the robust stability and robust performance characteristics of each closed-loop system are evaluated using μ. Since the environment around the vehicle is very complex, the uncertainty set will be treated as complex perturbations for a more conservative analysis.

$$\mathbf{\Delta}_C := \{\delta_1 : \delta_1 \in \mathbf{C}\}$$

The perturbation inputs/output from the frequency response is selected for a robust stability μ test. The input/output channels associated with the performance criterion are not used in the robust stability μ test.

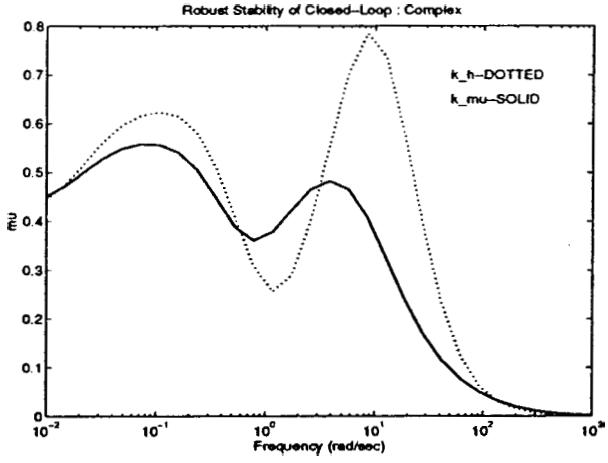

Figure 35: Robust Stability μ Analysis of k_h(dotted) and k_mu(solid)

As shown in Figure 35, the $KCmu$ controller has the better robust stability properties, when the perturbations are treated as complex (dynamic). The both peaks of the lower bound and the upper bound are approximately 0.55. It implies that. there is a complex perturbation of size $\frac{1}{0.55}$ that causes instability and for perturbations smaller than $\frac{1}{0.55}$ the closed-loop system

remains stable.

The appropriate block structure for the robust performance test is

$$\Delta_P := \{diag[\delta_1, \Delta_2]; \delta_1 \in \mathbf{R}, \Delta_2 \in \mathbf{C}^{7\times 6}\}$$

which is simply an augmentation of the real robust stability uncertain set with a complex 7×9 full block to include the performance objectives. Figure **36** shows the performance comparison of two controllers k_h and k_mu.

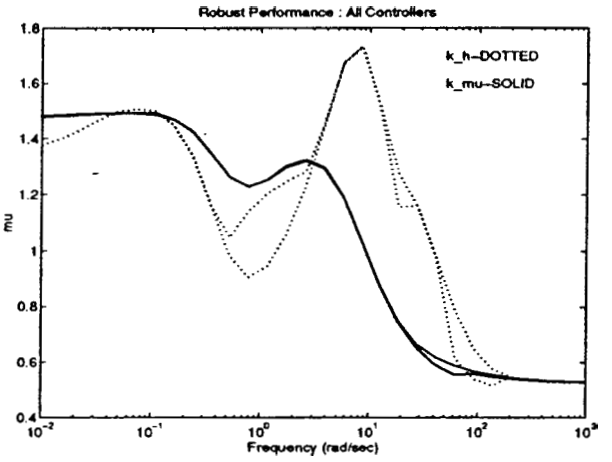

Figure **36:** Robust Performance μ Plots of k_h(dotted) and k_mu(solid)

4.6 Simulation Results

The robustness properties of two different controllers are investigated after implementing them into the PSP described in Section **2.** We chose here the same lead car velocity profile as that of in Section **3.1** so that our H_∞ contollers, k_h and k-mu, can be compared to the feedback linearization controller. Three controllers (Feedback Linearization, Robust H_∞ Controllers : k_h and k_mu) were compared for the above given condition. Figure **37** shows the velocity and spacing responses of vehicles in platoon under nominal conditions when the controller k_h is implemented. The responses for the controller k-mu under nominal conditions are shown in Figure **38.** The nominal responses for feedback linearization are given in Figure 9. It can be seen from these figures that the H_∞ controllers produce the tight spacing than feedback linearization. In order to examine the robustness to parameters, we assumed that the brake time constant of the second car is **0.3** and other cars are **0.2** (nominal value). Figures **39** and **40** show that the controllers k_h and k-mu improve the robustness with reasonable performance. Note that k_h and k-mu do not produce any

collisions, while the feedback linearization results in **an** intra-platoon collision between car1 and car2 (Figure **23).** Figures **38** and 40 show that the H_∞ controller designed with D – K iteration approach to p-synthesis guarantees **a** smaller spacing with ensured safety. Another merit of the H_∞ control approach is that all vehicles in the platoon have the same controller regardless of their position within the platoons. When the vehicle is located in the front of platoon, a feedback linearization approach causes the first vehicle to have different gains from other vehicles.

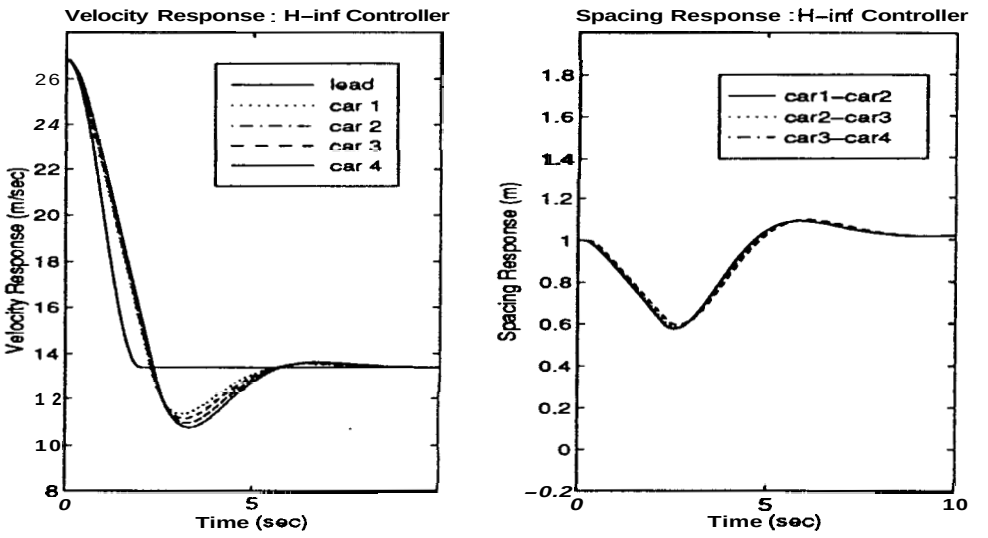

Figure **37:** H_∞ Controller : Velocity and Spacing Responses (Nominal Conditions)

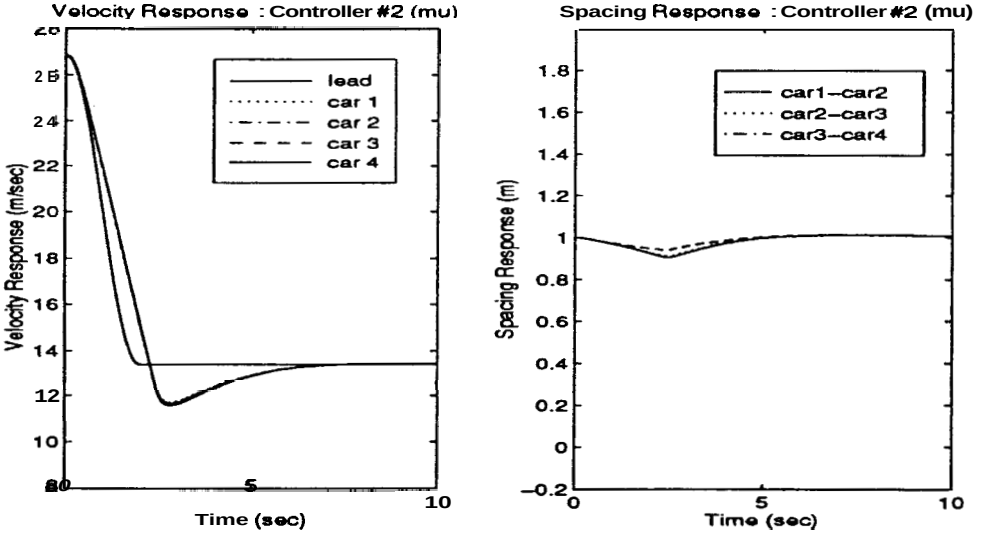

Figure **38:** Controller $\#2$ using μ : Velocity and Spacing Responses (Nominal Conditions)

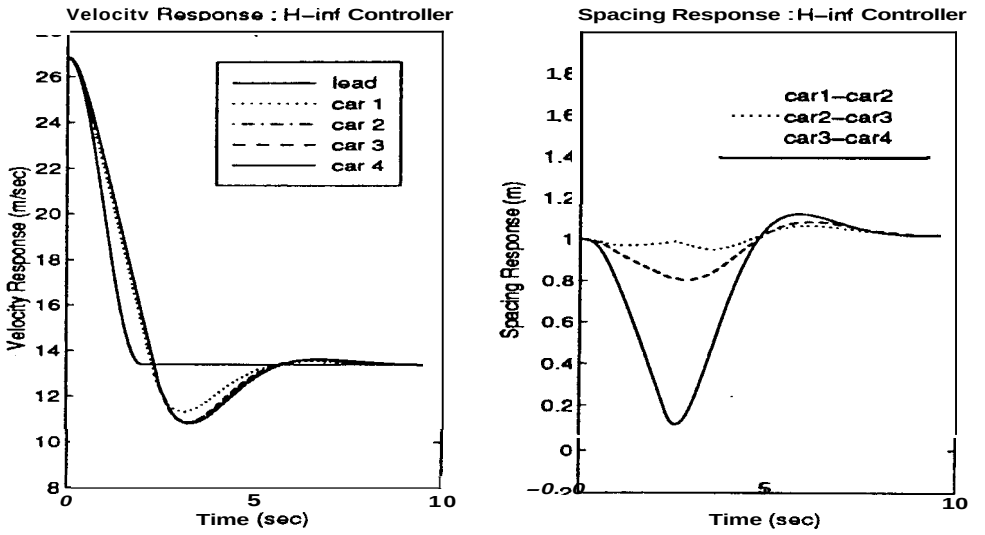

Figure **39:** H_∞ Controller : Velocity and Spacing Responses (When Car2 **Has** Worse Brake, $\tau_b = 0.3$)

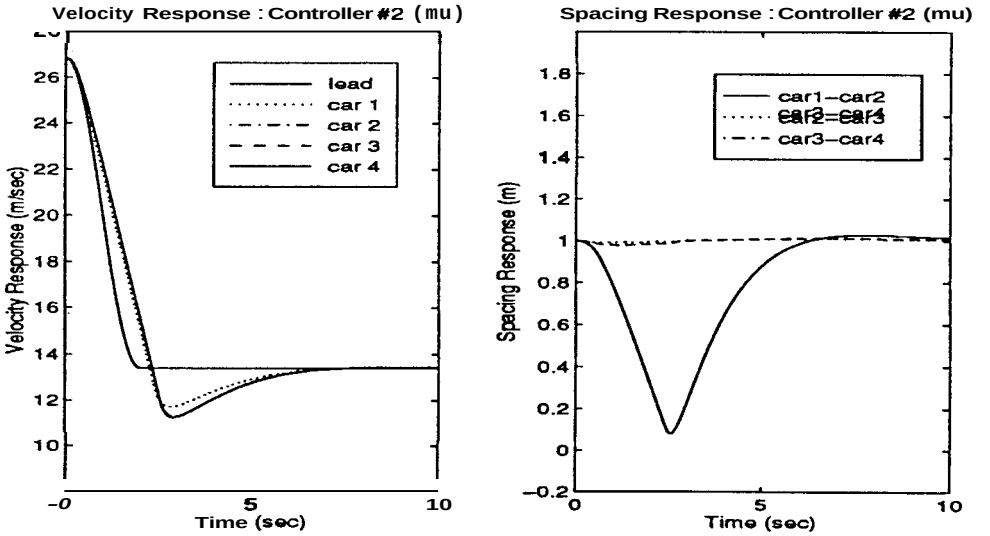

Figure 40: Controller #2 using μ : Velocity and Spacing Responses (When Car2 **Has** Worse Brake, $\tau_b = 0.3$)

5 Conclusions

The Collision Dynamics Module (CDM) has been integrated into the Platoon Simulation Package (PSP) as one of the refinements of the platoon simulation code. This gives us an analysis tool to analyze platoon dynamics under emergency collision situations. The modeling and physical analysis of platoon dynamics presented here appear to be reasonable and consistent with one's physical expectations.

The important question of here a platoon's dynamics will alter when non-uniform vehicles comprise the platoon has been addressed. At present, masses, engine and brake time constants are allowed to differ from their nominal values. The platoon's behavior was examined under the conditions of non-uniform brake time constant. In order to evaluate the platoon's behavior, minimum spacing and platoon length were computed.

An H_∞ optimization technique was developed to analyze and design the longitudinal controller of a vehicle of platoons in the face of parametric variations. An H_∞ controller was designed to optimize H_∞ performance, under the assumption of no model uncertainty, followed by a $D-K$ interation approach based on μ synthesis. From a parametric study of platoon dynamics considering brake time constant as the varying parameter, it was shown that both the H, controller and μ synthesis controller are robust, while feedback linearization may lead to intra-platoon collisions.

A Appendix

A.1 Preliminaries

In this section some mathematical preliminaries for H_∞ control theory and μ analysis/synthesis are presented. The proofs of theorems can be found in the corresponding references [1, 2, 9].

Definition **A.1 (Norms of** Signals **and** Systems) *For vector-valued signals,* $e(t) \in \mathbf{C}^n$, $e(t) = [e_1(t)\ e_2(t)\ \ldots\ e_n(t)]^T$, *the 1-, 2- and* ∞*-norms are defined as*

(1) 1-norm ($\mathcal{L}_1$ *norm)*

$$\| e \|_1 := \int_{-\infty}^{\infty} \| e(t) \| \, dt$$

(2) 2-norm ($\mathcal{L}_2$ *norm)*

$$\| e \|_2 := \left[\int_{-\infty}^{\infty} \| e(t) \|_2^2 \, dt \right]^{\frac{1}{2}}$$

(3) ∞*-norm* ($\mathcal{L}_\infty$ *norm)*

$$\| e \|_\infty := \sup_t \| e(t) \|_\infty$$

where $\mathcal{L}_1$, $\mathcal{L}_2$ *and* $\mathcal{L}_\infty$ *are Lebesgue spaces.*

The matrix H_2 *and* H_∞ *norm for the transfer matrix,* G, *are defined as*

(1) H_2 *norm*

$$\begin{aligned} \| G(j\omega) \|_2 &:= \left[\frac{1}{2\pi} \int_{-\infty}^{\infty} tr[G^*(j\omega)G(j\omega)] d\omega \right]^{\frac{1}{2}} \\ &= \left[\int_{-\infty}^{\infty} tr[g^*(t)g(t)dt \right]^{\frac{1}{2}} \\ &= \| g(t) \|_2 \end{aligned}$$

(2) H_∞ *norm* ($\mathcal{L}_\infty$ *space)*

$$\| G(j\omega) \|_\infty := \sup_{w \in \mathbf{R}} \bar{\sigma}[G(j\omega)]$$

(3) H_- *norm* (H_- *space)*

$$\| G(s) \|_\infty := \sup_{\mathrm{Re}(s)>0} \bar{\sigma}[G(s)]$$

where H_2 *and* H_- *are Hardy Spaces.*

Note that if G E H_∞ and rational, i.e. G is strictly stable (G E RH_∞),

$$\begin{aligned} \| G(s) \|_\infty &:= \sup_{\mathrm{Re}(s)>0} \bar{\sigma}[G(s)] \\ &= \sup_{w \in \mathbf{R}} \bar{\sigma}[G(j\omega)] \\ &=: \| G(j\omega) \|_\infty \end{aligned}$$

This is why the same symbol $\| \cdot \|_\infty$ is used in both $\mathcal{L}_\infty$ and H_∞ spaces.

Definition A.2 (Linear Fractional Transformation (LFT)) *Linear Fractional Transformations (LFT) are frequently used in H_∞ control synthesis and μ-Tools. They represent a standard way to unify the wide variety of feedback systems.*

(1) Lower LFT :

$$F_L(P,K) := P_{11} + P_{12}K(I - P_{22}K)^{-1}P_{21}$$

(2) Upper LFT :

$$F_U(P,\Delta) := P_{22} + P_{21}\Delta(I - P_{11}\Delta)^{-1}P_{12}$$

Note that $F_L(P,K)$ is the transfer function matrix from d to e, $e = F_L(P,K)d$, in Figure 41(a) and $F_U(P,\mathbf{A})$ is the transfer function matrix from d to e, $e = F_U(P,\Delta)d$, in Figure 41(b).

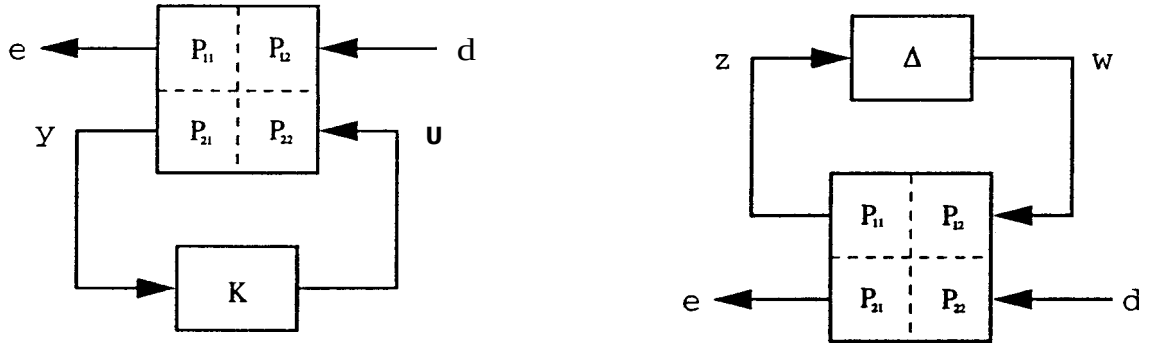

(a) Lower LFT (b) Upper LFT

Figure **41:** Linear Fiactional Transformations

Theorem A.1 (Small Gain Theorem) *Consider the feedback system in Figure 42. The system is internally stable if $\bar{\sigma}(P(j\omega)) \cdot \bar{\sigma}(K(j\omega)) < 1, \forall \omega \in \mathbf{R}$ assuming P, K are rational, proper and stable transfer functions ($P, K \in \mathcal{R}H_\infty$)*

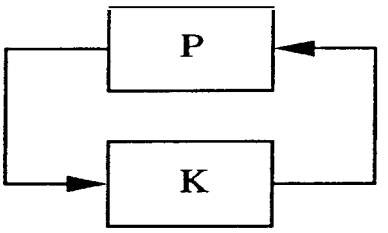

Figure **42:** Closed-loop System for Small Gain Theorem

This theorem states that if the loop gain is small, the closed loop stability is guaranteed. The Nyquist stability criterion can be used to justfy the validity of the single-input-single-output (SISO) version of this theorem. We should also note that the small gain theorem guarantees internal stability, i.e. all possible closed loop transfer functions are stable and all internal signals will remain bounded for bounded inputs.

A.1.1 H_∞ Control Theory

Theorem **A.2** (Robust Stability) *Consider a perturbed system which consists of a nominal plant (P) with a multiplicative uncertainty* **(A)** *as shown in Figure 43. A controller,* K, *stabilizes* $F_U(G, \mathbf{A})$ for *all permissible perturbations with* $\| \mathbf{A} \|_\infty \leq 1$ *iff*

(a) K stabilizes the nominal plant P

(b) $\| F_L(G, K) \|_\infty < 1$

where $G = \begin{bmatrix} 0 & W_u \\ P & P \end{bmatrix}$ *and* $F_L(G, K) = W_u K (I - PK)^{-1} P$

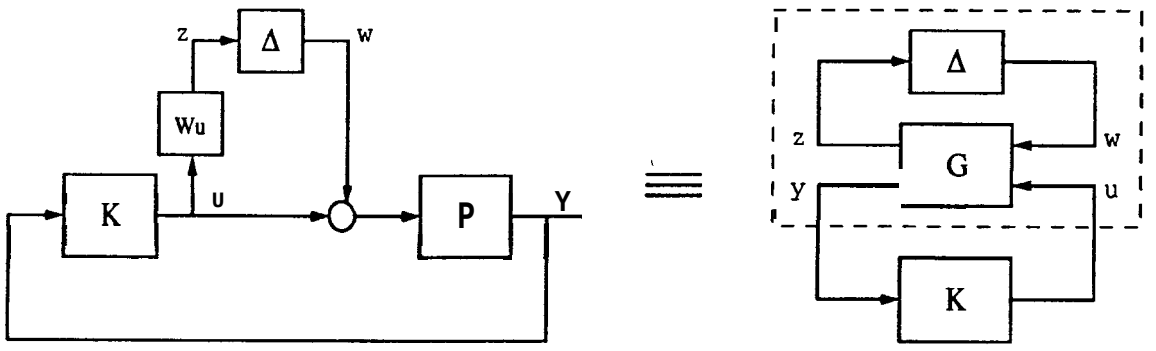

Figure **43:** Robust Stability **for** Perturbed Syatem with Multiplicative Uncertainty

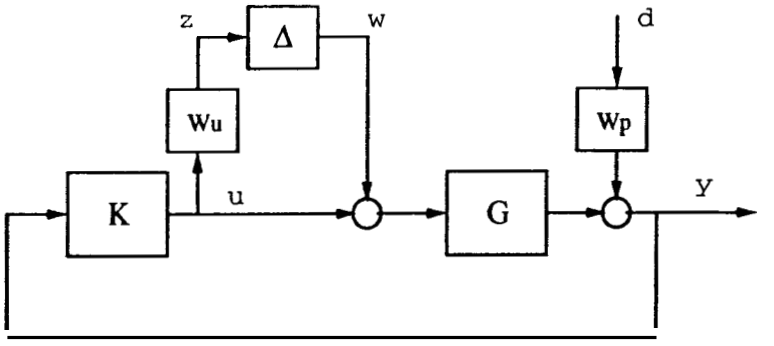

Figure 44: Mixed Sensitivity Problem

Theorem A.3 (Mixed Sensitivity Problem) *The mixed sensistivity problem is formulated as in Figure 44, where $G(s)$ is the transfer function of nominal plant, W_u and W_p are weighting functions and Δ represents multiplicative uncertainty model. The preformance and robustness objectives can be obtained simultaneously if a wntroller, $K(s)$, is designed to satisfy*

$$\left\| \begin{array}{c} W_u T(K) \\ W_p S(K) \end{array} \right\|_\infty < 1$$

where $T(K) = KG(I - KG)^{-1}$ and $S(K) = G(I - KG)^{-1}$. The robust stability can be achieved from $\|W_u T\|_\infty < 1$ and the disturbance (input noise) rejection can be specified by $\|W_p S\|_\infty < 1$.

H, Control Design Problem

Does there exist a linear controller, K, such that the closed loop system, e $= F_L(P,K)d$, is stable and $\|F_L(P,K)\|_\infty < \gamma$?

where $P = \begin{bmatrix} A & B_1 & B_2 \\ C_1 & D_{11} & D_{12} \\ C_2 & D21 & D_{22} \end{bmatrix} = \left[\begin{array}{cc} A & B \\ C & D \end{array} \right] = C(sI - A)^{-1}B + D$

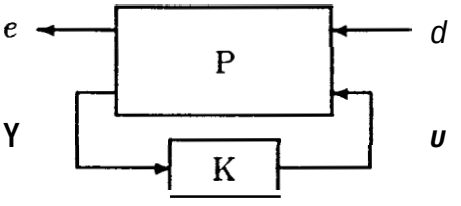

Assumptions

The following assumptions are required for output feedback.

(A1) (A,B_2) is stabilizable and (C_2,A) is detectable

(A2) D_{12} is full column rank and D_{21} is full row rank

(A3) $\begin{bmatrix} A - j\omega I & B_2 \\ C_1 & D_{12} \end{bmatrix}$ has full column rank for all w

(A4) $\begin{bmatrix} A - j\omega I & B_1 \\ C_2 & D_{21} \end{bmatrix}$ has full row rank for all w

Algorithm of Computing H_∞ norm in μ-tool

- Select of a positive number γ
- Test if $\|P\| < \gamma$ by calculating the eigenvalues of H (using $\|P\|_\infty < 1 \Leftrightarrow H$ has no eigenvalues on the imaginary axis)
  where $H := \begin{bmatrix} A + BR^{-1}D^*C & BR^{-1}B^* \\ -C^*(I - DD^*)^{-1}C & -(A + BR^{-1}D^*C)^* \end{bmatrix}$
  where $R = I - D^*D$
- Update γ based on the modified bisection algorithm
- Repeat

A.1.2 μ Analysis and Synthesis

Definition A.3 (Structured Singular Value) *For $M \in \mathbf{C}^{n\times n}$, $\mu_{\mathbf{\Delta}}(M)$ is defined*

$$\mu_{\mathbf{\Delta}}(M) := \frac{1}{min\{\bar{\sigma}(\Delta) : \mathbf{\Delta} \in \mathbf{A}, det(I - MA) = 0\}}$$

where $\mathbf{A} = \{diag[\delta_1 I_{r1}, \ldots, \delta_S I_{rs}, \Delta_1, \ldots, \Delta_F] : \delta_i \in \mathbf{C}, \Delta_j \in \mathbf{C}^{m_j \times m_j}\}$ (S and F represent the number of repeated scalar and full blocks, respectively). If there exist no $\mathbf{A} \in \mathbf{A}$ that makes $I - MA$ singular, define $\mu_{\mathbf{\Delta}}(M) := 0$.

Note that $\mu_{\mathbf{\Delta}}(\alpha M) = |\alpha|\mu_{\mathbf{\Delta}}(M), \forall \alpha \in \mathbf{C}$. However, the function $\mu : \mathbf{C}^{n\times n} \to \mathbf{R}$ is not a norm, since it does not satisfy the triangle inequality (i.e., $\mu_{\mathbf{\Delta}}(M + N) \not\leq \mu_{\mathbf{\Delta}}(M) + \mu_{\mathbf{\Delta}}(N)$).

Theorem A.4 (Robust Stability) *Let $\beta > 0$. The loop shown in below figure is well-posed and internally stable for all $\mathbf{\Delta} \in \mathbf{S}_{\mathbf{\Delta}} := \{\delta \in \mathbf{S} : \Delta(s_o) \in \mathbf{\Delta}, \forall s_o \in \bar{\mathbf{C}}_+\}$ with $\|\Delta\|_\infty < \frac{1}{\beta}$ iff*

$$\|M\|_{\mathbf{\Delta}} := \sup_{\omega \in \mathbf{R}} \mu_{\mathbf{\Delta}}(M(j\omega)) \leq \beta$$

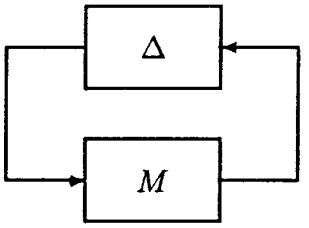

Theorem A.5 (Robust Performance) *Let* $\beta > 0$. *For all* $\Delta(s) \in \mathbf{S}_{\Delta}$ *with* $\|\Delta\|_\infty < \frac{1}{\beta}$, *the loop system below* is *well-posed, internally stable, and* $\|F_U(M,\Delta)\|_\infty \leq \beta$ *iff*

$$\|M\|_{\Delta_P} := \sup_{\omega \in \mathbf{R}} \mu_{\Delta_P}(M(j\omega)) \leq \beta$$

where $\Delta_p := \left\{ \begin{bmatrix} \Delta & \\ 0 & \Delta_F \end{bmatrix} : \mathbf{A} \in \mathbf{A}, \Delta_F \in \mathbf{C}^{n_d \times n_e} \right\}$, *in which* Δ_F is *augmented for performance.*

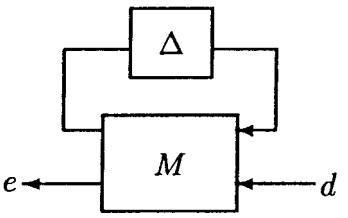

μ-Synthesis Control Problem

The standard p-synthesis problem (Figure 45) is to **find a controller,** K, **such that**

$$\max_{\omega} \mu_{\Delta}[F_L(P,K)(j\omega)] < 1$$

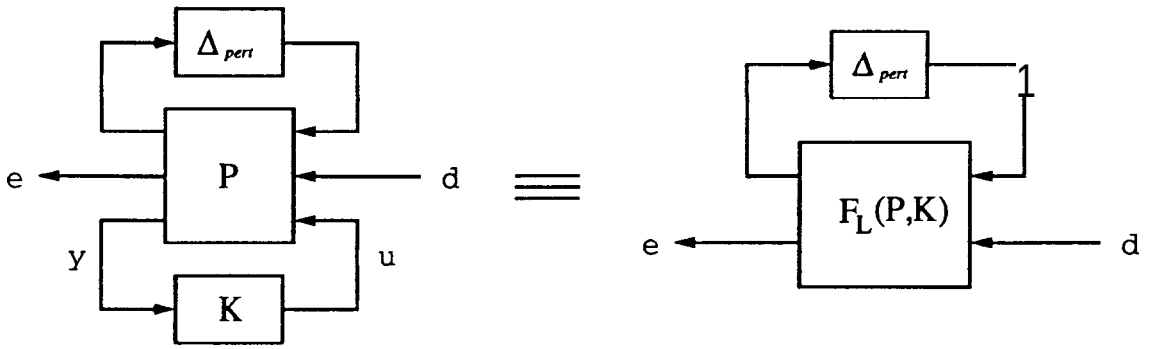

Figure 45: Closed-Loop View

The goal of p-synthesis is to minimize over all stabilizing controllers K, the peak value of $\mu_{\Delta}(\cdot)$ of the closed-loop transfer function $F_L(P,K)$, i.e.

$$\min_{stabilizing K} \max_{\omega} \mu_{\Delta}(F_L(P,K)(j\omega))$$

This is shown in below figure.

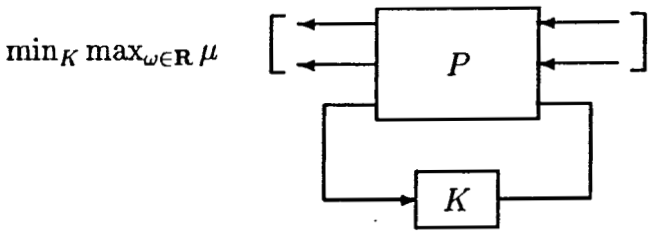

For tractability of the p-synthesis problem, it is necessary to replace $\mu_{\Delta}(\cdot)$ with the upper bound. The following properties can be used

$$\mu_{\Delta}(M) \leq \inf_{D \in \mathbf{D}_{\Delta}} \bar{\sigma}(DMD^{-1}) < 1$$

$$\Leftrightarrow \inf_{D \in \mathbf{D}_{\Delta}} \|DMD^{-1}\|_{\infty} < 1 \tag{32}$$

where $\mathbf{D}_{\Delta}$ is the set of matrices with the property that $D\Delta = \Delta D$, for every $D \in \mathbf{D}_{\Delta}$, $\mathbf{A} \in \mathbf{A}$. Hence, the new optimization is

$$\min_{\substack{K \\ stabilizing}} \quad \min_{\substack{\hat{D}(s) \in \mathbf{D} \\ stable, min-phase}} \quad \|\hat{D}F_L(P,K)\hat{D}^{-1}\|_{\infty} \tag{33}$$

This optimization is currently solved by an iterative approach, refered to as $D-K$ iteration. Note that μ problem becomes H_{∞} problem via $D-K$ iteration, which is described in above equations. A block diagram depicting the optimization is shown in Figure 46.

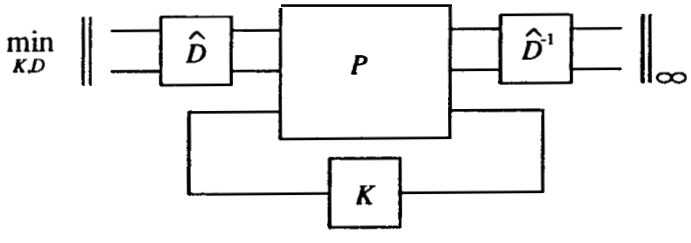

Figure 46: Replacing μ with Upper Bound

References

[1] A. Packard and J. Doyle, *The Complex Structured Singular Value,* Automatica, Vol. **29, No. 1,** pp **71-109, 1993.**

[2] Balas, Gary J., Doyle, John C., Glover, Keith, Packard, Andy, and Smith, Roy, *μ-Analysis and Synthesis Toolbox,* MUSYN Inc. and The Mathworks, Inc., January **1994.**

[3] Campbell, K.L., "Energy Basis for Collision Severity", Society of Automotive Engineers, Paper No. **740565.**

[4] Cho, D. and Hedrick, J. K., *Automotive Powertrain Modeling for Control,* Transactions ASME Journal of Dynamic Systems, Measurement, and Control, Vol. 111, No. **4,** December **1989.**

[5] Emori, R., "Analytical Approach to Automobile Collisions", Society of Automotive Engineers, Paper No. **680016.**

[6] Glimm, Jochen. and Fenton, E. R., *An Accident-Severity Analysis for a Uniform-Spacing Headway Policy,* IEEE Transactions on Vehicular Technology, Vol. VT-29, No. **1,** February **1980.**

[7] Hegmon, Rudolph R., *Tire-Pavement Interaction,* SAE Technical Paper Series **870241.**

[8] Hiltner, Edward; Arehart, Chuck; and Radlinski, Richard, *Light Vehicle ABS Performance Evaluation,* **US** Department of Transportation Final Report, DOT HS **807 813,** December **1991.**

[9] Kemin Zbou with John C. Doyle and Keith Glover, *Robust and Optimal Control,* Prentice Hall, **1995**

[10] Lu, X. P., "Effects of Road Roughness on Vehicular Rolling Resistance," *Measuring Road Roughness and Its Effects on User Cost and Comfort, ASTM STP 884,* T. D. Gillespie and Michael Sayers, Eds., American Society for Testing and Materials, Philadelphia, **1985,** pp. **143-161.**

[11] *MATLAB Reference Guide,* The Mathworks, Natick, Massachusetts, August **1992.**

[12] McMahon, Donn **H.** and Hedrick, J. Karl, *Longitudinal Model Development for Automated Roadway Vehicles,* PATH Research Report UCB-ITS-PRR-89-5, University of California at Berkeley, October **1989.**

[13] McMahon, D. H.; Hedrick, J. K.; and Shladover, S. E., *Vehicle Modeling and Control for Automated Highway System,* Proceedings of the **1990** American Control Conference, San Diego, CA, **1990.**

[14] NHTSA Research and Development Vehicle Crash Test Database, Available from Barbara C. Hennessy, NHTSA, U.S. Department of Transportation, 400 Seventh Street, S.W., Washington, D.C. 20590.

[15] Ramshaw, R. and Williams, T., *The Rolling Resistance of Commercial Vehicle Tyres*, Transport and Road Research Laboratory, Crowthorne, Berkshire, 1981.

[16] Reizes, H., *The Mechanics of Vehicle Collisions,* Charles C. Thomas, Springfield, Illinois, 1973.

[17] Sheikholeslam, Shahab and Desoer, Charles A., *Longitudinal Control of a Platoon of Vehicles I: Linear Model,* PATH Research Report UCB-ITS-PRR-89-3, University of California at Berkeley, August 18, 1989.

[18] Sheikholeslam, Shahab and Desoer, Charles A., *Longitudinal Control of a Platoon of Vehicles; II: First and Second Order Time Derivatives of Distance Deviations,* PATH Research Report UCB-ITS-PRR-89-6, University of California at Berkeley, December 1989.

[19] Sheikholeslam, Shahab and Desoer, Charles A., *Longitudinal Control of a Platoon of Vehicles; III: Nonlinear Model,* PATH Research Report UCB-ITS-PRR-90-1, University of California at Berkeley, April 1990.

[20] Sheikholeslam, Shahab and Desoer, Charles A., *Longitudinal Control of a Platoon of Vehicles,* ASME Journal of Dynamics, Control, and Measurement, June 1990

[21] Sheikholeslam, Shahab and Desoer, Charles A., *Longitudinal Control of a Platoon of Vehicles with no Communication of Lead Vehicle Information,* Proceedings of the American Control Conference, Vol. 3, 1991, pp. 3102-3106.

[22] Shladover, S. E., *Longitudinal Control of Automated Guideway Transit Vehicles Within Platoons,* ASME Journal of Dynamics, Control, and Measurement, vol. 100, December 1978, pp. 302-310.

[23] Shladover, S. E., *Longitudinal Control of Automotive Vehicles in Close-Formation Platoons,* ASME Journal of Dynamic Systems, Measurement, and Control vol. 113, June 1991, pp. 231-241.

[24] *SIMULINK User's Guide,* The Mathworks, Inc., Massachusetts, March 1992.

[25] Smith, C. G.; McGehee, D. Y.; and Healey, A. J., *The Prediction of Passenger Riding Comfort from Acceleration Data,* ASME Journal of Dynamic Systems, Measurement, and Control, vol. 100, March 1978, pp. 34-41.

[26] Strother, C.E, Woolley, R.L., and James, M.B., *A Comparison Between NHTSA Crash Test Data and CRASH3 Frontal Stiffness Coefficients*, Society of Automotive Engineers Paper No. 900101.

[27] Strother, C.E, Woolley, R.L., James, M.B., and Warner, C.Y., *Crush Energy in Accident Reconstruction,* Society of Automotive Engineers, Paper No. 860371.

[28] Swaroop, D. **V.** A. **H.** G., *String Stability of Interconnected Systems: An Application to Platooning in Automated Highway Systems,* Ph.D. Thesis, Vehicle and Dynamics Laboratory, University of California at Berkeley, 1994

[29] Tongue, Benson H.; Moon, Ahrie; and Harriman, Douglas, ***Low** Speed Collision Dynamics: Second Year Report,* PATH Research Report, University of California at Berkeley, 1996.

[30] Tongue, Benson H.; Packard, Andy; and Sachi, Paul, *Qualitative Analysis on the Performance of Non-uniform Platoons: Report I, Non-uniformities and Performance Issues,* PATH Research Report, University of California at Berkeley, 1997.

[31] Tongue, Benson H.; Packard, Andy; and Sachi, Paul, *Qualitative Analysis on the Performance of Non-uniform Platoons: Report II, Worst Case Platoon Performance,* PATH Research Report, University of California at Berkeley, 1997.

[32] Tongue, Benson H.; Packard, Andy; and Harriman, Douglas, *A Vehicle Collision Model for Platoon Controller Development,* PATH Research Report, University of California at Berkeley, 1997.

[33] Tongue, Benson H.; Yang, Yean-Tzong; and White, Matthew T., *Platoon Collision Dynamics and Emergency Maneuvering I: Reduced Order Modeling of a Platoon for Dynamical Analysis,* PATH Research Report UCB-ITS-PRR-91-15, University of California at Berkeley, August 1991.

[34] Tongue, Benson H. and Yang, Yean-Tzong, *Platoon Collision Dynamics and Emergency Maneuvering II: Platoon Simulations for Small Disturbances,* PATH Research Report UCB-ITS-PRR-94-4, University of California at Berkeley, February 1994.

[35] Tongue, Benson H. and Yang, Yean-Tzong, *Platoon Collision Dynamics **and** Emergency Maneuvering III: Platoon Collision Models and Simulations,* PATH Research Report UCB-ITS-PRR-94-02, University of California at Berkeley, February 1994.

[36] Tongue, Benson H. and Yang, Yean-Tzong, *Platoon Collision Dynamics and Emergency Maneuvering IV: Intra-Platoon Collision Behavior and **a** New Control Approach **for** Platoon Operation During Vehicle Exit/Entry - Final Report,* PATH Research Report UCB-ITS-PRR-94-25, University of California at Berkeley, November 1994.